Null-like and Time-like Geodesics Near Static and Rotating Black Holes

by

Mancini Matteo Emmanuele

School of Engineering, Computing and Mathematics
University of Plymouth
England
15/04/2024

Abstract

This study investigates the behaviour of particle trajectories in the vicinity of the Schwarzschild (static) and Kerr (rotating) black holes (both uncharged), focusing on both light-like (for photons) and time-like geodesics (for massive particles). Understanding the motion of particles in the gravitational field of black holes is fundamental and applicable to many astrophysical phenomena and theories, including the Penrose process. We aim to educate how the geometry of spacetime around black holes influences the motion of particles with different energy and angular momentum. Utilising the framework of general relativity, we employ numerical integration methods, including Runge- Kutta 4 and EinsteinPy (a Python package used to compute numerical integration through FANTASY), to solve the geodesic equation governing the motion of test particles in the space-time metric for both static and rotating black holes. Including various scenarios, such as particles falling radially towards the event horizon and stable orbits at different distances. Our result analysis shows a clear difference between particle with the same initial parameters but orbiting two different black holes. As the static black hole is spherically symmetric, angular momentum is conserved, hence the particle stays on a planar orbit, while for rotating black holes, due to frame dragging effect, particles manifest non-planar orbits. Additionally, for the null-like geodesics we can observe gravitational deflection and photosphere. These findings contribute to our understanding of gravitational phenomena in extreme astrophysical environments and have implications for interpreting observational data from black hole systems.

Acknowledgments

I would like to thank my supervisor, Dr Craig McNeile, whose wide knowledge and experience in the field of General Relativity provided guidance throughout this project. I would also like to thank the following people, who supported me throughout the whole degree! To all of my family members, in particular my mother, Stella Amodio, for believing in me when nobody else did, my father, Gesumino Mancini, for his patient and wise advice, my co-father, German Cuartas, for his support and to Riccardo and Lorenzo for being the best brothers anyone can dream of. To all the people outside my family, Professor David McMullan, for being a true rule model and guide, Dr Davide Vadacchino and Dr Ben King, even with their busy schedules, they consistently make time to warmly welcome and assist me.

Contents

Chapter 1

Introduction

A black hole[85] is a region of spacetime[83], predicted from Einstein's theory of general relativity[85], where its gravity is so intense that nothing can escape it, including photons. This prediction was observed in the physical universe, making black holes one of the many predictions from general relativity that were confirmed years later, through several experiments[101]. Before we provide further details on black holes, we require to analyse some key concept of the theories of special and general relativity. Chapters 2 and 3 cover all the background required from special and general relativity, to be able to develop the mathematical tools required understand black holes and their properties. The concept of black hole is covered in Chapter 4, providing all the background required for the purpose of this project and the different structures of static (Schwarzschild [39, 96]) and rotating (Kerr [10, 90]) black holes, we are not interested to charged black holes as it goes beyond the scope of this thesis. Chapter 5 contains all the work done to numerically solve the light-like and time-like geodesics for the Schwarzschild and Kerr spacetime, together with plots of the results obtained given different initial conditions to the problem. At the end of this chapter there is a comparison of particle trajectories derived from a specific set of initial conditions, applied to both static and rotating black holes. The numerical methods utilised to numerically integrate geodesics are Runge-Kutta 4, see Chapter 5 section 5.1.1, and FANTASY, see Chapter 3 section 3.3. All the conclusions are presented in Chapter 6. Note throughout the paper you will find hyperlinks that will take you to my GitHub page, containing all the codes used to produce the provided plots (see my GitHub page).

Chapter 2

Background of Special Relativity

This chapter contains all the relevant mathematical tools to solve relativistic problems of this project, starting with special relativity to then move on to general relativity.

2.1 Principles of Special Relativity

Special relativity (SR), was published on 26 September 1905 by Albert Einstein[1], in a paper on the Electrodynamics of Moving Bodies. This fundamental theory of physics revolutionised our comprehension of space and time, where in Galilean relativity space and time are separated (they are each other absolute). So the main feature of SR is the replacement of the Newtonian mechanics and Galilean transformations with the Lorentz transformation, where time and space are not separated but these are joined into a single continuum defined as spacetime[2]. At the core of SR there are two postulates (from which lead to several counter-intuitive phenomena confirmed through experiments):

1. ***The principle of relativity:*** *the laws of physics, including electromagnetism, are the same in all inertial frames.*

2. ***The principle of invariant speed of light:*** *every observer measures the same value c (= 299 792 458 m/s) for the speed of light (in vacuum[3]) in all inertial frames.(for more information, look for [51])*

Before proceeding, it is important to define the following;
An **observer** is an individual or a system capable of perceiving and recording information about the physical world. For the scope of this thesis, we consider an observer as a **reference frame**, which is a system of coordinates used to describe the position and the motion of a particle (or more general object).
By definition, an **inertial frame** is an observer that is not affected by acceleration, i.e. the observer can be moving at a constant velocity (time independent) and still considered inertial. For SR an inertial frame is simply a spacetime coordinate system, in which the location $\vec{x} = (x, y, z)$ is recorded at a time (t) of any event. These coordinate systems for inertial frames (inertial observers) must satisfy the following three properties:

[1] not just Einstein but also other brilliant minds contributed to the formulation of SR, Hendrik Lorentz, Henri Poincaré and Hermann Minkowski who published his work on spacetime in 1907

[2] In theoretical physics and cosmology, spacetime is a model used to describe our universe in terms of three special dimensions, often denoted as $\vec{x} = (x, y, z)$, and one temporal dimension, denoted as t.

[3] a vacuum (or vacua) is a space void of matter, e.g. gas, liquid and solid particles

1. The distance between two points, say P_1 (coordinates x_1, y_1, z_1) and P_2 (coordinates x_2, y_2, z_2), is time independent.

2. Within an inertial frame all clocks at every point of the frame are synchronised and ticking off the same time coordinate t.

3. In inertial frames for a constant time t, the geometry of space is Euclidean. This property is very important as it simplifies calculations that would be more challenging in presence of gravity (see general relativity).

Framework, in relativity frame work refers to a mathematical and theoretical structure where physical phenomena are recorded and analysed, among this mathematical tools for a deep understanding of black holes physics and structure, one requires *time dilatation* and *length contraction* (more mathematical tools will be provided for general relativity).
An **event**, is anything that occurs at precise location at a specific time, i.e. a location in spacetime.

2.1.1 Relativistic Time Dilatation

To provide a description of what time dilatation is, let us consider two inertial frames, one static (not moving) denoted by $\mathcal{O}$, coordinates t, x, y, z, and one moving (at constant velocity, v) denoted by $\bar{\mathcal{O}}$, coordinates $\bar{t}, \bar{x}, \bar{y}, \bar{z}$. Also, consider $\mathcal{O}$ (the static frame) as our reference frame. In each frame there is a clock, the moving frame, $\bar{\mathcal{O}}$, will experience a relativistic time dilatation, in particular $\bar{\mathcal{O}}$'s clock will result to be slower (this can be either a minor or drastic difference in time dilatation, depending on how fast $\bar{\mathcal{O}}$ is moving respect to $\mathcal{O}$) compared to $\mathcal{O}$'s clock.
One can derive the time dilatation equation through a simple thought experiment, to be consistent with the above description, our reference frame $\mathcal{O}$ can be described as two fixed parallel mirrors located at position P_1 and P_2. Between the two a light ray is emitted and it starts "bouncing" from P_1 to P_2 and then back to P_1, the mirrors are separated by a distance L. For the moving frame $\bar{\mathcal{O}}$ the mirrors are still located at the point P_1 and P_2, but here the mirrors are both moving at the same constant velocity v, the physical distance between P_1 and P_2 remains the same L, but now the light ray travels at a diagonal distance D. Let us define each distance in terms of the time required to travel from P_1 to P_2 and back to P_1 for both frames, Δt (static) and $\Delta \bar{t}$ (moving).

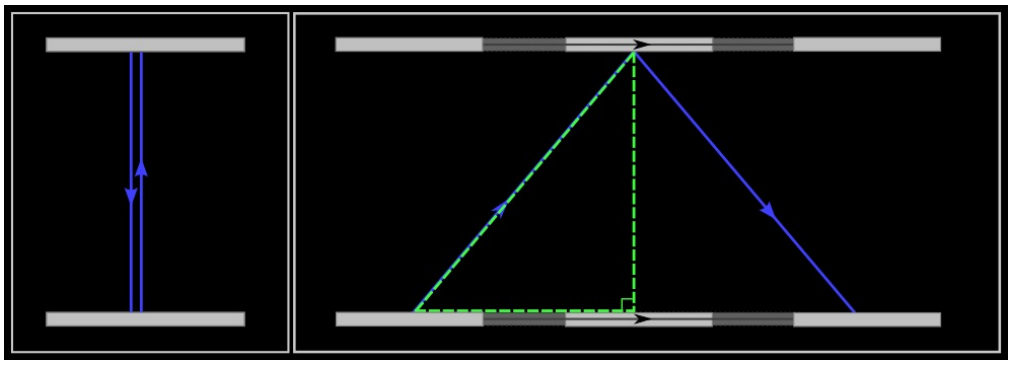

Figure 2.1: Representation of the above description, on the left the rest frame and on the right the moving frame. The blue lines are the trajectories of the light ray.

With the above information, one can derive the time dilatation equation. From the left picture:

$$\Delta t = 2\frac{L}{c} \tag{2.1.1.1}$$

In equation 2.1.1.1 c is the speed of light, and $2L$ is the distance covered by the light ray. From the picture on the right one can derive the two following equations:

$$\Delta \bar{t} = 2\frac{D}{c} \tag{2.1.1.2}$$

Using the Pythagoras theorem:

$$D^2 = \left(\frac{1}{2}v\Delta\bar{t}\right)^2 + L^2 \tag{2.1.1.3}$$

In equation 2.1.1.3, the term $\frac{1}{2}v\Delta\bar{t}$ is the distance travelled from the photon[1] from position P_1 to position P_2 with respect to P_1 in $\bar{\mathcal{O}}$ (in other words the leg aligned with P_1).
Now one can rearrange equations 2.1.1.1 and 2.1.1.2 to make L and D the subject of the equation:

$$\left(\frac{\Delta\bar{t}c}{2}\right)^2 = \left(\frac{\Delta\bar{t}v}{2}\right)^2 + \left(\frac{\Delta tc}{2}\right)^2$$

Dividing through $\frac{c^2}{4}$:

$$(\Delta\bar{t}c)^2 = \left(\Delta\bar{t}\frac{v}{c}\right)^2 + (\Delta t)^2$$

Rearrange take $\Delta\bar{t}$ terms to both sides, factorise and divide through to obtain the *time dilatation equation*[41],

$$\Delta\bar{t} = \frac{\Delta t}{\sqrt{1-\frac{v^2}{c^2}}} = \gamma\Delta t \tag{2.1.1.4}$$

where γ is the Lorentz factor[2].
For a complete introduction in SR and time dilatation consider [41, 85].

2.1.2 Length Contraction

Length contraction, also known as the Lorentz contraction, is a phenomenon that occurs when the length of a moving object appears to be less than its actual length in a rest frame. The equation of the length contraction is given by:

$$L = \frac{L_0}{\gamma} \tag{2.1.2.1}$$

where:

- L is the length registered by a moving inertial frame relative to an object in a rest frame.
- L_0 is the actual length of the object in the rest frame.
- γ is the Lorentz factor. (see previous section 2.1.1)

[1] A photon is a fundamental particle of light and electromagnetic radiation. This elementary particle shows both wave-like and particle-like properties.

[2] Named after the Hendrik Lorentz, the Lorentz factor (or gamma factor), is a quantity used to measure the change of time and length of an object while moving. We will encounter this many more times. *More can be fount in [103].*

From the above, it is quite evident that to experience length contraction, one should move at a considerable fraction of the speed of light. This shows, in day-to-day life no one experiences length contraction, as not sufficient speed is achieved. Furthermore, length contraction only occurs in the direction of the moving object.
For more information about the derivation of the length contraction eq. see papers [15] [52].

2.1.3 Lorentz Transformation

Consider a particle moving at constant velocity v, on a straight line trajectory, with the absence of external forces, one can measure, for example, its velocity in spacetime with respect to an specific frame, $\mathcal{O}$ (reference frame). Now another measurement, of the particle's velocity, is registered in another frame, $\bar{\mathcal{O}}$. The particle's intrinsic[1] properties are the same in all frames, regardless of these properties, the measurements collected from the two frames will differ from each other, this is because the two frames have different coordinate orientations. The disagreement between the two frames can be caused from many factors, including time dilatation and length contraction. The conversion from one frame to the other is known as *Lorentz transformations*, which consists of a group of six-parameter of linear transformations that preserves spacetime intervals between two events. This transformations include three rotations and three boosts (known as Lorentz boosts, these are a change in velocity) along different spacial directions. (*Deriving all the transformations is beyond the scope of this thesis, for more information on Lorentz transformations see [58].*)

The most common Lorentz transformation is the "simple" boost, parameterised by the above velocity v, along the x-direction of $\mathcal{O}$. This can be expressed by the following transformation:

$$\begin{aligned} \bar{t} &= \gamma\left(t - \frac{vx}{c^2}\right), \quad \bar{y} = y \\ \bar{x} &= \gamma\left(x - vt\right), \quad \bar{z} = z \end{aligned}$$

where the coordinates (t, x, y, z) and $(\bar{t}, \bar{x}, \bar{y}, \bar{z})$ of $\mathcal{O}$ and $\bar{\mathcal{O}}$, respectively. γ is the Lorentz factor and c is the speed of light in a vacuum. The above transformation can be rewritten as the following;

$$\begin{aligned} c\bar{t} &= \gamma\left(ct - \beta x\right), \quad \bar{y} = y \\ \bar{x} &= \gamma\left(x - \beta ct\right), \quad \bar{z} = z \end{aligned}$$

where $\beta = \frac{v}{c}$. *See more on simple boosts in Chapter 1 of A First Course in General Relativity[85]*

2.2 Introduction to Tensors in SR

The particle's intrinsic and physical properties are the same in all frames, regardless of these properties, the measurements collected in the two different frames will differ from each other In this section a brief review of vectors is provided, then we are going to move on to tensors, in particular the metric, and tensors differentiation.

2.2.1 Vectors Review, Contravariant and Covariant Vectors

Background and Notation

[1] A particle intrinsic properties, are independent of external forces, e.g. mass is unchanged under the action of external forces.

In physics, one can describe the position of a particle using *vectors* (not just position, but other important quantities, such as velocity, acceleration, momentum and more). A vector is a quantity with direction and magnitude, denoted by components of a coordinate system, such as Cartesian, Polar and Spherical.

Depending on the literature, one can find different ways to denote a vector. Here we will denote vectors as $\vec{x} = (t, x, y, z)$, this is also know as a **four-vector**[1]. Let us denote the *basis vector*[2] as the following:

$$\vec{e}_0 = (1, 0, 0, 0),$$
$$\vec{e}_1 = (0, 1, 0, 0),$$
$$\vec{e}_2 = (0, 0, 1, 0),$$
$$\vec{e}_3 = (0, 0, 0, 1).$$

Another important notation that will be used is $\vec{x} = x^\alpha \vec{e}_\alpha$ (upper index[3]) where $\alpha = 0, 1, 2, 3$. Here we have adopted the Einstein summation convention, where the sum is embedded within the index i.e.

$$\vec{x} = \sum_{\alpha=0}^{3} x^\alpha \vec{e}_\alpha \equiv x^\alpha \vec{e}_\alpha \tag{2.2.1.1}$$

therefore $\vec{x} = x^0\vec{e}_0 + x^1\vec{e}_1 + x^2\vec{e}_2 + x^3\vec{e}_3 = (x^0, x^1, x^2, x^3) \equiv (t, x, y, z)$. *For more information on vectors, use of notation and vector algebra, see Chapter 2 of A First Course in General Relativity[85].*

The notation used above to describe a vector and its components, is known as ***contravariant*** vector, where the components *contra-vary* with a change of basis. The matrix responsible for transforming the vector components must be the inverse of the matrix that transforms the vector itself, i.e. $\vec{x} = x^\alpha \vec{e_\alpha}$.

The dual[4] of a contravariant vector is known as the ***covariant*** vector (covector), here the components *co-vary* with a change of basis. Covectors are denoted as $\vec{x} = x_\alpha \vec{e}^\alpha$.

2.2.2 Minkowski Space and the Metric Tensor

Minkowski Space
On September 21, 1908, Hermann Minkowski, during one of his lectures of the title "space and time", he presented an alternative formulation of spacetime to what Henri Poincaré's paper in relativity, published in 1905, where he showed that by considering time to be an imaginary fourth spacetime coordinate, denoted as ict where c is the constant speed of light in a vacuum and $i = \sqrt{-1}$ i.e. (ict, x, y, z), the Lorentz transformations can be interpreted as rotations of Euclidean sphere in four dimensions.
Alternatively Minkowski formulation considers the idea of using a real-time coordinate instead of

[1] A four-vector is a mathematical object that describes a physical quantity in spacetime, which transforms under Lorentz transformations.

[2] Basis vectors are a set of independent vectors that span a vector space

[3] Note, upper index is not a power, $(x^0)^2$ here 0 is the index and 2 is the power

[4] For any vector space V there exists a corresponding dual vector space, which consists of all linear forms on V, including point-wise addition and scalar multiplication. *See Dual Vector spaces[75].*

the imaginary used from Poincaré, representing the four variables of spacetime as (t, x, y, z). In nowadays, the notation used and studied is the one of Minkowski space.

Structure of Minkowski Space
In the previous section on vectors 2.2.1, we introduced the notation and structure of vectors for the scope of this project, for Minkowski space, the same basis vectors are utilised here, i.e. $\vec{e}_\alpha$. The particular observation here, is that the inner-product (IP) between two vectors will have signature $(+,-,-,-)$ (in many books also $(-,+,+,+)$). For instance, consider the following example, define the four-dimensional vector $\vec{x} = (ct, x, y, z)$, its modulus square is given by $(\vec{x})^2 = c^2t^2 - x^2 - y^2 - z^2 \equiv c^2t^2 - r^2$, where $\vec{r} = (x, y, z)$ is the position vector in $\mathbb{R}^3$. *For more information on Minkowski space, see [100], and for more about Henri Poincaré see[63].*
From the above it follows that, a vector:

- is **time-like** if $c^2t^2 > r^2$
- is **space-like** if $c^2t^2 < r^2$
- is **light-like** if $c^2t^2 = r^2$

This is expressed as $\eta(\vec{x}, \vec{x})$, where η is the metric tensor, with zero entries everywhere except the diagonal entries, which are $(1, -1, -1, -1)$.

The metric tensor
In differential geometry, the metric tensor (or simply metric) is a mathematical object that defines the geometry of manifolds[1], in particular the distance and angles between points in the manifold. In the terms of general and special relativity, the metric describes the local geometry of spacetime.
Notation: as already mentioned, the metric tensor is denoted by the Greek letter η, which is used to denote the inner product between pairs of tangent vectors.
Consider the two vectors $\vec{A} = A^\alpha \vec{e_\alpha}$ and $\vec{B} = B^\beta \vec{e_\beta}$, their inner product is given by:

$$\vec{A} \cdot \vec{B} = (A^\alpha \vec{e_\alpha}) \cdot \left(B^\beta \vec{e_\beta}\right)$$

$$= A^\alpha B^\beta \, (\vec{e_\alpha} \cdot \vec{e_\beta})$$

where the metric is defined as $\eta_{\alpha\beta} = (\vec{e_\alpha} \cdot \vec{e_\beta})$, where $\eta_{00} = 1$ and $\eta_{ij} = -\delta_{ij}$, here δ_{ij} is the Kronecker delta, hence the IP between $\vec{A}$ and $\vec{B}$ is,

$$\vec{A} \cdot \vec{B} = A^\alpha B^\beta \eta_{\alpha\beta} \tag{2.2.2.1}$$

Equation 2.2.2.1 is often denoted as $\eta(\vec{A}, \vec{B}) = A^\alpha B^\beta \eta_{\alpha\beta}$, by expanding 2.2.2.1, i.e. $\vec{A} \cdot \vec{B} = A^0B^0 - A^1B^1 - A^2B^2 - A^3B^3$ one can see that it is consistent with the definition of the Minkowski spacetime.

A matrix representation of $\eta_{\alpha\beta}$:

$$\eta = \begin{bmatrix} 1 & 0 & 0 & 0 \\ 0 & -1 & 0 & 0 \\ 0 & 0 & -1 & 0 \\ 0 & 0 & 0 & -1 \end{bmatrix} \tag{2.2.2.2}$$

[1] A manifold is a topological space that locally resembles Euclidean space near each point.

Note, until now we have encountered different indices denoted by either Greek or Latin letters, each of them have different ranges, Latin letters are used to denote only space in $\mathbb{R}^3$, e.g. $i = 1, 2, 3$. While Greek letters denote spacetime, e.g. $\alpha = 0, 1, 2, 3$. *For more information about the metric see Chapter 3 of A First Course in General Relativity[85]*

2.2.3 Four-momentum and its Conservation

Four-velocity

Before we get to the *four-momentum* it is important to introduce the *four-velocity*. Recall, in classical mechanics the momentum is define as the rate of change in position of a particle time its mass, i.e. $p = mv$ in $\mathbb{R}$ where p is the momentum, m the mass of the particle and v its velocity.
In the Galilean space and time, the momentum is represented as $p^i = mv^i$ $(i = 1, 2, 3)$, where v^i is the tangent vector to the particle's path. While in four-geometry spacetime we define $\vec{U} = U^\alpha$ as our *four-velocity to be the tangent vector to the world line*[1] *of the particle*. The magnitude square of a four-velocity, by applying the the metric $\eta_{\alpha\beta}$, is always equal to the speed of light square, c^2 (depending on the choice of metric, it can also take the value of $-c^2$), that is:

$$U^\alpha U_\beta = U^\alpha U^\beta \eta_{\alpha\beta} = c^2 \tag{2.2.3.1}$$

Now consider equation 2.1.1.4, from section 2.1.1, we had $\Delta\bar{t} = \gamma\Delta t$, where γ is the Lorentz factor, $\bar{t}$ and t are time coordinates of two different inertial frames. By relabeling $\bar{t}$ as t (left hand side), and t as τ (right hand side) denoting the proper time[2], then we can rewrite the time dilatation equation as $\Delta t = \gamma\Delta\tau$, from this it follows that:

$$dt = \gamma(v)d\tau \tag{2.2.3.2}$$

where the Lorentz factor γ is a function of the Euclidean norm of the vector $\vec{v}$ in $\mathbb{R}^3$, i.e. $v^2 = (v^1)^2 + (v^2)^2 + (v^3)^2$.
Let $\vec{X}(\tau)$ be the four-position, then the four-velocity $\vec{U}$ at any point in the world line is denoted as:

$$\vec{U} = \frac{d\vec{X}}{d\tau} \tag{2.2.3.3}$$

Four-velocity Components

One can explicitly break down equation 2.2.3.3, to determine each component of the four-vector. One can recall the relationship between the time t and the coordinate x^0, defined as $x^0 = ct$, one can then take the derivative with respect to the proper time τ, provides the following result:

$$U^0 = \frac{dx^0}{c\tau} = c\frac{dt}{d\tau}$$

using the relationship stated in equation 2.2.3.2, the above reduces to:

$$U^0 = c\gamma(v) \tag{2.2.3.4}$$

repeating the same process for the other components (velocity components) U^i for $i = 1, 2, 3$:

$$U^i = \frac{dx^i}{d\tau}$$

[1] A world line is the path traced by an object through four-dimensional spacetime, representing its entire history from past to future.

[2] Proper time is the time interval measured by a clock in a rest frame.

using the chain rule,

$$\frac{dx^i}{d\tau} = \frac{dx^i}{dt}\frac{dt}{d\tau}$$

using equation 2.2.3.2, where $\frac{dx^i}{dt} = u^i$ and $\frac{dt}{d\tau} = \gamma(v)$, one obtains:

$$U^i = \gamma(v)u^i \tag{2.2.3.5}$$

Thus, in equations 2.2.3.5 and 2.2.3.4, we found the components of the four-velocity, and now we can denote it as $\vec{U} = \gamma(c, \vec{u})$. As we defined and derived the four-velocity and its components, we can now move on to four-momentum.

Four-momentum
As you would expect the four-momentum is defined as:

$$\vec{p} = m\vec{U} \tag{2.2.3.6}$$

where m is the *rest mass*[3], and $\vec{U}$ is the four-velocity. This, generalise the three-dimensional momentum in classical mechanics to a four-dimensional momentum in spacetime. The components of a four-momentum are the following:

$$\vec{p} = (p^0, p^1, p^2, p^3) = (\frac{E}{c}, p^i) \tag{2.2.3.7}$$

Where we define p^0 as the energy of the particle, in a frame, denoted by E. The norm square of the four-momentum is known as the Minkowski norm, this gives a Lorentz invariant[4] quantity,

$$p^\alpha p_\beta = p^\alpha p^\beta \eta_{\alpha\beta} = \frac{E^2}{c^2} - \delta_{ij}p^i p_j = m^2c^2 \tag{2.2.3.8}$$

Conservation of Four-momentum
In classical mechanics the interaction of a system of particles is governed by the laws of conservation of energy and momentum. As the four-momentum components reduces to a non-relativistic limit, Galilean-like energy and momentum, it is necessary to postulate the relativistic law so that the four-momentum is conserved in the world line. The conservation of four-momentum due to the interaction of several particles can be expressed by the following sum:

$$\sum_i p_i^\alpha = constant \tag{2.2.3.9}$$

where p_i^α represent the four-momentum of the i^{th} particle in the system. The conservation of four-momentum arises from the invariance of physical laws under translations in spacetime, *first postulate of SR.* (*For more information on the four-velocity see [86], and for four-momentum and its conservation see [71] and [14] also see chapter 2 of A First Course in General Relativity [85]*).

2.3 Tensors

We already encountered the metric tensor in the two previous sections (2.2.2 and 2.2.3), but we have not yet defined what a tensor is.

[3]Rest mass refers to the intrinsic mass of an particle when it is at rest relative to a moving frame
[4]Lorentz invariant quantity, is invariant under the Lorentz transformation

2.3.1 Definition and Properties of Tensors

A tensor is a powerful tool that generalise the concept of scalar quantities, vectors and matrices to higher-dimensional space, precisely one can think of a tensor as a multi-dimensional array of numerical values that obey particular transformation rules under a change of coordinate system, this emphasises the importance of tensors in SR and GR. There are several type of tensors (but we will be only looking at the most relevant tensors for GR). Tensors can be classified on their rank[1], which is the number of indices required to specify each component of a tensor.
For example if we consider the two tensors T^i_j and T_{ij}, they both are rank 2 tensors as they have two indices, but they have different meanings. If we recall the definition covariant and contravariant, one can see that T^i_j has both covariant and contravariant indices, while T_{ij} has two covariant indices. This leads us to the following definition:

- A $(0, N)$ tensor, is a N rank tensor with N covariant indices.
- A $(M, 0)$ tensor, is a M rank tensor with M contravariant indices.
- A (M, N) tensor, is a $M + N$ rank tensor with N covariant and M contravariant indices.

Essentially, covariant indices are denoted with subscripts and contravariant indices with superscript. In SR and GR we will be mainly dealing with tensors of rank 2.
A $(0, 1)$ tensor is known as **one-form** (or covector at a point), one form are denoted with a subscript index, as an example the vector x_α is a type of one-form, whose basis are $\vec{e}^\alpha$. One-forms map vectors to scalars, these are particularly important for differential geometry.

2.3.2 Tensor Algebra

The simplest operations are *addition* and *subtraction* of tensors, however, for two tensors in order to be added or subtracted, they need to be of the same rank and structure in terms of component. Considering the two tensors mentioned in the above section (2.3.1), namely T^i_j and T_{ij}, these two tensors can neither be added nor subtracted, regardless of their common rank, as these tensors have different components (compare to addition and subtraction of matrices. For this to be possible both matrices have to be of the same dimension).
What is more relevant and, at the same time, less trivial is the tensor product, contraction, raising and lowering index.

Tensor product, denoted by the symbol $\otimes$, takes two tensors and maps them to another tensor, whose rank is the sum of the ranks of the original tensors. For examples if one computes a tensor product between two one-forms then the map is a (0, 2) tensor. Tensor product has the following properties:

1. The tensor product is **bilinear**, meaning it is linear in its arguments. That is, for tensors A, B and C and the scalars k, l, the following property hold: $(kA) \otimes B = k(A \otimes B)$.
2. The tensor product is **associative**: $(A \otimes B) \otimes C = A \otimes (B \otimes C)$.
3. **Distributive** over tensor addition:$(A + C) \otimes B = A \otimes B + C \otimes B$.
4. **Mixed Products**: tensor product allows for combining tensors of different types (e.g. vectors and co-vectors). For example, if v^α is a vector and w_β is a co-vector, their tensor product $v^\alpha \otimes w_\beta$ result to be a rank 2 tensor, a (1, 1) to be precise.

[1]Note also the terms degree and order are used.

5. **Component Product**: consider the two matrices A, a $i \times j$ matrix, and B, a $l \times k$ matrix, then their tensor product $A \otimes B$ is an $il \times jk$ matrix.

Tensor contraction is an operation performed on tensor(s) where one index is summed over while the corresponding components are multiplied. This operation effectively reduces the rank of the tensor. Suppose we have a (M, N) tensor, when contracted it reduces to a $(M-1, N-1)$, hence the rank of the contracted tensor is $M + N - 2$ (reduced by two). Consider the two following examples of contraction:

- Consider the tensor T^i_{jkl}, this is a (1, 3) tensor, if one performs the contraction $i \to j$, i.e. $T^i_{jkl} \to T^j_{jkl} = S_{kl}$, where the tensor S_{kl} is a contraction of T^i_{jkl}. This is referred as contraction of the indices i and j.
- Contraction can be used to determine the **trace** of a tensor. Consider the tensor A^i_j and B_{lk}, by contracting indices i and j for A^i_j, and indices l and k for B_{lk}, this provides the two traces (scalars) A^j_j and B_{kk}, which correspond to the sum of the diagonal elements of each tensor.

Raising and lowering an index of a tensor is performed by contracting the tensor with a metric tensor. In GR it is often done to switch between covariant and contravariant representation of the tensor. We have already encountered the metric as $\eta_{\alpha\beta}$, in section 2.2.2, let us now denote $\mathbf{g}$ as our metric tensor, such that the operation $\mathbf{g}(\vec{e}_\alpha, \vec{e}_\beta) = \eta_{\alpha\beta}$, hence we can say that $\mathbf{g}$ acts like a map, in particular the it can be expressed as a map of vectors into one-forms. The metric $\mathbf{g}$ is both symmetric and invertible, these are really important properties, hence one can also map a one-form to a vector using the inverse of the metric. The inverse of the metric is denoted with covariant indices, i.e. $\eta^{\alpha\beta}$ is the invesre of $\eta_{\alpha\beta}$. This can also be extended to higher order tensors, thus it can map an (M, N) tensor to an $(M-1, N+1)$ or an $(M+1, N-1)$ tensor. Other than renaming the tensor, one can keep the same name, but distinguish the contraction or change of indices only by the position of the indices. Given the components of a (1, 2) tensor namely $T^\alpha_{\beta\gamma}$ then one can:

- **raise** an index,
$$T^{\alpha\beta}_\gamma = \eta^{\beta\mu} T^\alpha_{\mu\gamma} \tag{2.3.2.1}$$
by applying the metric inverse obtaining a (2, 1) tensor,
- **lower** an index,
$$T_{\alpha\beta\gamma} = \eta_{\alpha\mu} T^\mu_{\beta\gamma} \tag{2.3.2.2}$$
by applying the metric obtaining a (0, 3) tensor.

Performing raising or lowering of indices in tensor calculus ensures consistent notation, facilitates correct transformation under coordinate changes, and supports physical interpretation, therefore it enhance the clarity and efficiency of calculations in GR.
Furthermore, it is possible to compute *mixed component of a metric*, as already stated $\eta_{\alpha\beta}$ are the components of the metric, and $\eta^{\alpha\beta}$ are the components of its inverse. Now by combining the components of the metric and its inverse, the result is the mixed components of the metric, i.e.

$$\eta^\alpha_\beta \equiv \eta^{\alpha\mu}\eta_{\mu\beta} \tag{2.3.2.3}$$

Looking at the right hand side, one can notice that we are computing the product of two matrices that are each others inverse, hence the result must be the identity matrix, as previously seen denoted by the Kronecker delta, therefore:

$$\eta^\alpha_\beta \equiv \delta^\alpha_\beta \tag{2.3.2.4}$$

2.3.3 Tensor Calculus

Differentiation of Tensors

As in calculus and vector calculus, where one can take the derivative of a function or calculate the curl of a vector field, it is possible to compute the derivative of a tensor with respect to its components. However, we need to be cautious when taking the derivative of a tensor, as we need to consider its components and how they are transformed under changes of coordinates. This differentiation can be done using partial derivatives, covariant derivatives and other appropriate differential operators.
A function f is a (0, 0) tensor, when computing its gradient, i.e. ∇f ($\equiv dx_\alpha f$ index notation), one obtains a vector field, a one-form, a (0, 1) tensor. This shows that, by differentiating a function it produces a tensor of one higher rank, in particular higher covariant.
Let us consider the (1, 1) tensor $\mathbf{T}$, whose components, $T^\alpha_\beta = T^\alpha_\beta \vec{e}^\beta \otimes \vec{e}_\alpha$, are functions of position dependent on the parameter τ (proper time). To determine the rate of change with respect to τ, we proceed as follows:

$$\frac{d\mathbf{T}}{d\tau} = \left(\frac{dT^\alpha_\beta}{d\tau}\right) \vec{e}^\beta \otimes \vec{e}_\alpha \tag{2.3.3.1}$$

Where $dT^\alpha_\beta/d\tau$ is an ordinary derivative along the word line. By the chain rule this simplify to:

$$\frac{dT^\alpha_\beta}{d\tau} = \frac{\partial T^\alpha_\beta}{\partial x^\gamma}\frac{dx^\gamma}{d\tau} = T^\alpha_{\beta,\gamma} U^\gamma \tag{2.3.3.2}$$

here $T^\alpha_{\beta,\gamma}$ is a short hand notation for $\partial T^\alpha_\beta/\partial x^\gamma$, where γ represent the component that we are differentiating for, and U^γ are the components of the four-velocity vector $\vec{U}$. Hence, by collecting everything together:

$$\frac{d\mathbf{T}}{d\tau} = \left(T^\alpha_{\beta,\gamma}\vec{e}^\beta \otimes \vec{e}_\alpha\right) U^\gamma \tag{2.3.3.3}$$

From equation 2.3.3.3, we can deduce an important result, the *gradient* of $\mathbf{T}$:

$$\nabla\mathbf{T} := T^\alpha_{\beta,\gamma}\vec{e}^\beta \otimes \vec{e}^\gamma \otimes \vec{e}_\alpha \tag{2.3.3.4}$$

Tensors and tensor fields are very important, here we have summarised the most relevant information for the purpose of this thesis, all the information provided about tensors can be found in [30, 54] and Chapter 3 of A First Course in General Relativity [85].

2.4 Connection to General Relativity

Special relativity laid the foundation for a profound shift in our understanding of space, time, and motion. It introduced revolutionary concepts such as time dilation, length contraction, and the equivalence of mass and energy, reshaping our notions of the fundamental nature of the universe (we have already met few of these concepts in this chapter). Building upon the principles of special relativity (see section 2.1), Einstein later developed general relativity in 1915. General relativity extends the principles of special relativity to include accelerated frames of reference and gravitational effects. By positing that mass and energy warp the fabric of space-time, general relativity provides a geometric description of gravity, where the curvature of space-time determines the paths that objects follow. Thus, while special relativity addresses the behaviour of objects in the absence of gravitational fields and at constant velocities, general relativity broadens this framework to include the effects of gravity and accelerated motion, offering a more comprehensive understanding of the fundamental nature of the cosmos.

Chapter 3

Background of General Relativity

The transition from special to general relativity is not trivial. In synthesis what Einstein provided in SR is an adaptation of Newton's laws of motion for electrodynamics, along with new concepts of space and time. However, these concepts were inconsistent with the Newtonian theory of gravity, this led Einstein, between 1907 and 1915, to the formulation of general relativity (GR), which is a theory of gravitation, that states *"the gravitational effect between two bodies results from the deformation of spacetime, due to the presence of their masses"*. This was revolutionary, as for more than two hundred years the Newtonian laws of gravitation were accepted as a valid description of gravitational interaction between bodies. Despite the unknown nature of gravity, Newton's model is quite accurate for basic frameworks to describe body motions.

A good example where Newton's law of motion fails is the orbit of Mercury, where through experiments and observations showed the consistency of Einstein's description of gravity, taking in consideration several factors impacting the orbit of Mercury such as minutes anomalies. Furthermore, GR models gravitational effects such as gravitational waves, gravitational lensing and gravitational time dilatation.

Einstein derived his theory of GR from the **equivalence principle**[28, 29, 85], which is a fundamental concept in physics stating that the effects of gravity are indistinguishable from those of acceleration. In particular, Einstein started to question whether an observer in a free falling elevator would be able to detect gravitational force. As a result, the observer would not be able to feel the force of gravity. Instead, they would feel weightless, just as if they were in a region of space with no gravity at all. This led Einstein to conclude that there is no fundamental difference between the effects of gravity and the effect of acceleration.
When Einstein realised that gravity and acceleration were equivalent, then mass must somehow curve the fabric of spacetime, this is known as **curved spacetime**[19, 83, 85], resulting in one of the major changes from the geometry of spacetime in SR, where spacetime is asymptotically flat, to its geometry in GR. Hence, objects moving through curved spacetime would appear to be influenced by gravity. This lead to many important results, such as **geodesic principle**[68, 79] and **field equation**[35].

In this chapter we will provide a background of GR that is particularly relevant for the **Penrose process**[11, 57, 77, 93], highly relevant for the energy extraction process from a rotating Black hole.

3.1 Spacetime Geometry

We have already encountered spacetime and some of its key concepts and applications in SR, where the Minkowski space 2.2.2 models flat spacetime. In GR, due to the presence of gravity, spacetime is curved. To model this, a geodesic[1] is required. Before, we derive the Geodesic equation, it is require the use of some machinery tools, in particular the Christoffel symbol and covariant derivative.

3.1.1 The Christoffel Symbol

The Christoffel symbol[53, 85], denoted by $\Gamma^{\alpha}_{\beta\gamma}$, represent the components of the connection on a manifold. They describe how coordinate bases change as one moves from point to point on the manifold, serving as coefficients in the covariant derivative of vector fields. In essence, they quantify the geometric properties of the manifold and are crucial in defining the covariant derivative, which incorporates the curvature of the space.

Christoffel Symbol in Terms of the Metric
Previously we denoted the metric as $\mathbf{g}(\vec{e}_\alpha, \vec{e}_\beta) \equiv \eta_{\alpha\beta}$[85], we will now use $g_{\alpha\beta}$ as a short hand notation for $\mathbf{g}(\vec{e}_\alpha, \vec{e}_\beta)$. Now let's consider our first definition for the Christoffel symbol. Suppose we have the vector $\vec{e}_\alpha$, by computing its derivative one obtains: $\frac{\partial \vec{e}_\alpha}{\partial x^\beta}$, which is also a vector, whose components are $\frac{\partial e_\alpha}{\partial x^\beta}$. By introducing the Christoffel symbol, one can rewrite $\frac{\partial \vec{e}_\alpha}{\partial x^\beta}$ as the following:

$$\frac{\partial \vec{e}_\alpha}{\partial x^\beta} = \Gamma^{\mu}_{\alpha\beta}\vec{e}_\mu \tag{3.1.1.1}$$

where $\Gamma^{\mu}_{\alpha\beta}$ is the μ^{th} component of $\frac{\partial \vec{e}_\alpha}{\partial x^\beta}$. Interpretation of indices:

- (α) is the basis vector being differentiated.
- (β) gives the coordinates with respect to which it is being differentiated.
- (μ) are the components of the resulting derivative.

To write the Christoffel symbol in terms of the metric, one can take the scalar product of equation 3.1.1.1, with another basis vector $\vec{e}_\nu$, also consider the above definition of the metric $g(\vec{e}_\alpha, \vec{e}_\beta) = g_{\alpha\beta}$ then:

$$\Gamma^{\mu}_{\alpha\beta}\vec{e}_\mu \cdot \vec{e}_\nu = \frac{\partial \vec{e}_\alpha}{\partial x^\beta} \cdot \vec{e}_\nu - \frac{\partial \vec{e}_\nu}{\partial x^\beta} \cdot \vec{e}_\alpha$$

$$\Gamma^{\mu}_{\alpha\beta} g_{\mu\nu} = \frac{\partial}{\partial x^\beta} g_{\alpha\nu} - \Gamma^{\mu}_{\nu\beta}\vec{e}_\mu \cdot \vec{e}_\alpha = g_{\alpha\nu,\beta} - \Gamma^{\mu}_{\nu\beta} g_{\mu\alpha}$$

Where in $g_{\alpha\nu,\beta}$ is a short hand notation for $\frac{\partial}{\partial x^\beta} g_{\alpha\nu}$. By now rearranging:

$$g_{\alpha\nu,\beta} = \Gamma^{\mu}_{\alpha\beta} g_{\mu\nu} + \Gamma^{\mu}_{\nu\beta} g_{\mu\alpha} \tag{3.1.1.2}$$

Here μ is the "dummy" index, while α, β and ν are specified. By permutation of the indices, one can obtain the following two equations:

$$g_{\alpha\beta,\nu} = \Gamma^{\mu}_{\alpha\nu} g_{\mu\beta} + \Gamma^{\mu}_{\beta\nu} g_{\mu\alpha} \tag{3.1.1.3}$$

$$g_{\nu\beta,\alpha} = \Gamma^{\mu}_{\nu\alpha} g_{\mu\beta} + \Gamma^{\mu}_{\beta\alpha} g_{\mu\nu} \tag{3.1.1.4}$$

[1] In GR, a geodesic describes the notion of a straight line to curved spacetime, this is covered in 5.1.0.1

Now consider the symmetric property of the Christoffel symbol, i.e. $\Gamma^{\mu}_{\alpha\beta} = \Gamma^{\mu}_{\beta\gamma}$, one can then add equations 3.1.1.2 and 3.1.1.3 and subtract equation 3.1.1.4, this gives the following result:

$$g_{\alpha\nu,\beta} + g_{\alpha\beta,\nu} - g_{\nu\beta,\alpha} = \Gamma^{\mu}_{\alpha\beta} g_{\mu\nu} + \Gamma^{\mu}_{\nu\beta} g_{\mu\alpha} + \Gamma^{\mu}_{\alpha\nu} g_{\mu\beta} + \Gamma^{\mu}_{\beta\nu} g_{\mu\alpha} - (\Gamma^{\mu}_{\nu\alpha} g_{\mu\beta} + \Gamma^{\mu}_{\beta\alpha} g_{\mu\nu})$$

this simplifies to;

$$2\Gamma^{\mu}_{\nu\beta} g_{\mu\alpha} = g_{\alpha\nu,\beta} + g_{\alpha\beta,\nu} - g_{\nu\beta,\alpha}$$

By recalling the inverse of a metric i.e. $(g_{\mu\alpha})^{-1} = g^{\mu\alpha}$, and applying it to both sides and dividing by two, we obtain:

$$\Gamma^{\mu}_{\nu\beta} = \frac{1}{2} g^{\mu\alpha} (g_{\alpha\nu,\beta} + g_{\alpha\beta,\nu} - g_{\nu\beta,\alpha}) \tag{3.1.1.5}$$

This is the Christoffel symbol in terms of the metric.

3.1.2 The Christoffel Symbol in Spherical Coordinates (3D)

In this section we will compute the Christoffel symbol in spherical coordinates (3D). The calculation provided and the results are obtained through manual computation, hence one can verify if the output of the code provided in python[1], that uses the einsteinpy[2] package, agrees with the manual computation. In spherical polar coordinates (r, θ, ϕ), the metric g_{ij} (here denoting indices with Latin letters is appropriate since we are in 3D) is defined as follows:

$$g_{ij} = \begin{bmatrix} 1 & 0 & 0 \\ 0 & r^2 & 0 \\ 0 & 0 & r^2 \sin^2\theta \end{bmatrix} \tag{3.1.2.1}$$

while its inverse, g^{ij}, is given by:

$$g^{ij} = \begin{bmatrix} 1 & 0 & 0 \\ 0 & \frac{1}{r^2} & 0 \\ 0 & 0 & \frac{1}{r^2 \sin^2\theta} \end{bmatrix} \tag{3.1.2.2}$$

This is a lengthy calculation, hence a full working procedure is provided for only one of the components of the Christoffel symbol, but results for the rest of the components will be provided. Is important to notice that the off diagonal elements of the metric and its inverse are zero, hence $g_{ij} = g^{ij} = 0$ for $i \neq j$. Recall equation 3.1.1.5, let's now compute $\Gamma^{r}_{\theta\theta}$ and $\Gamma^{\theta}_{r\phi}$.

Computation of $\Gamma^{r}_{\theta\theta}$:

$$\begin{aligned} \Gamma^{r}_{\theta\theta} &= \frac{1}{2} g^{rr} (g_{r\theta,r} + g_{r\theta,\theta} - g_{\theta\theta,r}) \\ &= \frac{1}{2}(1)(0 + 0 - \frac{\partial}{\partial r}(-r^2)) \\ \Gamma^{r}_{\theta\theta} &= -\frac{2r}{2} = -r \end{aligned}$$

[1]Python is a versatile programming language known for its simplicity, readability, and wide range of applications.
[2]This will be introduced section 5.1.0.1

Computation of $\Gamma^{\theta}_{r\phi}$:

$$\begin{aligned}\Gamma^{\theta}_{r\phi} &= \frac{1}{2}g^{\theta\theta}(g_{\theta r,\phi} + g_{\theta\phi,\theta} - g_{r\phi,\theta}) \\ &= \frac{1}{2r^2}(0+0-0) \\ \Gamma^{\theta}_{r\phi} &= 0\end{aligned}$$

If one repeats the same procedure for different permutations of r, θ and ϕ, resulting into the following:

- $\Gamma^{r}_{\phi\phi} = -r\sin^2\theta$
- $\Gamma^{\theta}_{r\theta} = \Gamma^{\theta}_{\theta r} = \frac{1}{r}$
- $\Gamma^{\phi}_{r\phi} = \Gamma^{\phi}_{\phi r} = \frac{1}{r}$
- $\Gamma^{\phi}_{\theta\phi} = \Gamma^{\phi}_{\phi\theta} = \frac{\cos\theta}{\sin\theta} = \cot\theta$

These are the non-zero Christoffel symbol in spherical polar coordinates. They reflect the curvature of the space described by these coordinates. See the link to Christoffel symbol in spherical polar coordinates.

3.1.3 Geodesic Equation

The geodesic equation is a fundamental concept in differential geometry and GR. In essence, it describes the path followed by a free-falling object in curved spacetime, where "free-falling" means moving without being subject to any non-gravitational forces [68, 79]. There are many ways one can derive the geodesic equation, among those we find derivation of the geodesic equation through **action**[1] **principle**[26].

Derivation Through Action Principle
To proceed one can think of a geodesic between two **timelike**-separated events, i.e. the two events are separated but follow the same time. Let S be the action between the two events, such that $S = \int ds$, where $ds = \sqrt{-g_{\alpha\beta}(x)dx^{\alpha}dx^{\beta}}$ is the line element, as the curve is timelike the sign inside the square root is negative by definition, (see Minkowski space section 2.2.2). By varying the action S, one can derive the geodesic, starting with the introduction of the parameter ζ, we can parameterise S. Therefore,

$$S = \int d\zeta \sqrt{-g_{\alpha\beta}\frac{dx^{\alpha}}{d\zeta}\frac{dx^{\beta}}{d\zeta}}$$

By the application of the **principle of least action**[87], i.e. $\delta S = 0$, we vary the action path with respect to x^{α}. In our case,

$$\delta S = 0 = \int d\zeta \delta\left(\sqrt{-g_{\alpha\beta}\frac{dx^{\alpha}}{d\zeta}\frac{dx^{\beta}}{d\zeta}}\right) = \int d\zeta \frac{\delta\left(-g_{\alpha\beta}\frac{dx^{\alpha}}{d\zeta}\frac{dx^{\beta}}{d\zeta}\right)}{2\sqrt{-g_{\alpha\beta}\frac{dx^{\alpha}}{d\zeta}\frac{dx^{\beta}}{d\zeta}}}$$

[1] An action is a scalar quantity that describes how energy changes with respect to time on a physical system.

Now by applying the chain rule, we have:

$$0 = \int d\zeta \left(\delta g_{\alpha\beta} \frac{dx^\alpha}{d\zeta} \frac{dx^\beta}{d\tau} + g_{\alpha\beta} \frac{d\delta x^\alpha}{d\zeta} \frac{dx^\beta}{d\tau} + g_{\alpha\beta} \frac{dx^\alpha}{d\tau} \frac{d\delta x^\beta}{d\zeta} \right)$$

$$= \int d\zeta \left(\frac{dx^\alpha}{d\zeta} \frac{dx^\beta}{d\tau} \frac{\partial}{\partial x^\mu} g_{\alpha\beta} \delta x^\mu + 2 g_{\alpha\beta} \frac{d\delta x^\alpha}{d\zeta} \frac{dx^\beta}{d\tau} \right)$$

where $\frac{d\tau}{d\zeta} = \sqrt{-g_{\alpha\beta} \frac{dx^\alpha}{d\zeta} \frac{dx^\beta}{d\zeta}}$, also we have eliminated the negative sign. At the boundaries the total derivative is equal to zero, hence we can "drop" it, and applying integration by parts,

$$0 = \int d\tau \left(\frac{dx^\alpha}{d\tau} \frac{dx^\beta}{d\tau} \frac{\partial}{\partial x^\mu} g_{\alpha\beta} \delta x^\mu - 2\delta x^\alpha \frac{d}{d\tau} \left(g_{\alpha\beta} \frac{dx^\beta}{d\tau} \right) \right)$$

$$= \int d\tau \left(\frac{dx^\alpha}{d\tau} \frac{dx^\beta}{d\tau} \frac{\partial}{\partial x^\mu} g_{\alpha\beta} \delta x^\mu - 2\delta x^\alpha \frac{\partial}{\partial x^\mu} g_{\alpha\beta} \frac{dx^\mu}{d\tau} \frac{dx^\beta}{d\tau} - -2\delta x^\alpha g_{\alpha\beta} \frac{d^2 x^\beta}{d\tau^2} \right)$$

$$= \int d\tau \delta x^\alpha \left(-2 g_{\alpha\beta} \frac{d^2 x^\beta}{d\tau^2} + \frac{dx^\mu}{d\tau} \frac{dx^\beta}{d\tau} \frac{\partial}{\partial x^\alpha} g_{\mu\beta} - 2 \frac{dx^\mu}{d\tau} \frac{dx^\beta}{d\tau} \frac{\partial}{\partial x^\mu} g_{\alpha\beta} \right)$$

$$= \int d\tau \delta x^\alpha \left(-2 g_{\alpha\beta} \frac{d^2 x^\beta}{d\tau^2} + \frac{dx^\mu}{d\tau} \frac{dx^\beta}{d\tau} \frac{\partial}{\partial x^\alpha} g_{\mu\beta} - \frac{dx^\mu}{d\tau} \frac{dx^\beta}{d\tau} \frac{\partial}{\partial x^\mu} g_{\alpha\beta} - \frac{dx^\beta}{d\tau} \frac{dx^\mu}{d\tau} \frac{\partial}{\partial x^\beta} g_{\alpha\mu} \right)$$

Now divide both sides by -2,

$$0 = \int d\tau \delta x^\alpha \left(g_{\alpha\beta} \frac{d^2 x^\beta}{d\tau^2} + \frac{1}{2} \frac{dx^\mu}{d\tau} \frac{dx^\beta}{d\tau} \left(\frac{\partial}{\partial x^\mu} g_{\alpha\beta} + \frac{\partial}{\partial x^\beta} g_{\alpha\mu} - \frac{\partial}{\partial x^\alpha} g_{\mu\beta} \right) \right)$$

for the above integral to be zero, we must have that,

$$0 = g_{\alpha\beta} \frac{d^2 x^\beta}{d\tau^2} + \frac{1}{2} \frac{dx^\mu}{d\tau} \frac{dx^\beta}{d\tau} \left(\frac{\partial}{\partial x^\mu} g_{\alpha\beta} + \frac{\partial}{\partial x^\beta} g_{\alpha\mu} - \frac{\partial}{\partial x^\alpha} g_{\mu\beta} \right) \tag{3.1.3.1}$$

by applying the inverse of the metric to both sides of equation 3.1.3.1, i.e. $g^{\alpha\lambda}$ we obtain the following;

$$0 = \frac{d^2 x^\lambda}{d\tau^2} + \frac{1}{2} g^{\alpha\lambda} \left(\frac{\partial}{\partial x^\mu} g_{\alpha\beta} + \frac{\partial}{\partial x^\beta} g_{\alpha\mu} - \frac{\partial}{\partial x^\alpha} g_{\mu\beta} \right) \frac{dx^\mu}{d\tau} \frac{dx^\beta}{d\tau} \tag{3.1.3.2}$$

using the Christoffel symbol, equation 3.1.3.2 simplifies to,

$$0 = \frac{d^2 x^\lambda}{d\tau^2} + \Gamma^\lambda_{\mu\beta} \frac{dx^\mu}{d\tau} \frac{dx^\beta}{d\tau} \tag{3.1.3.3}$$

where equation 3.1.3.3 is the geodesic equation.

3.1.4 Riemann Curvature Tensor

In this section we are going to cover, briefly, Riemannian manifolds [85] and their curvature[102], before introducing the Riemann curvature tensor[85].

A differentiable manifold hosting a symmetric (0, 2) tensor field **g**, designated as a metric at every location is defined a **Riemannian manifold**. Note how the choice of metric affects the structure of the manifold itself, by defining its curvature. For example as we shall see the Schwarzschild metric[85, 96] is adopted to represent spherical bodies such as stars and non-rotating black holes. A common way to denote this is with the map:

$$\mathbf{g}\left(\frac{\partial}{\partial x^{\alpha}}, \frac{\partial}{\partial x^{\beta}}\right) : U \to \mathbb{R} \tag{3.1.4.1}$$

for any 'smooth' choice of metric **g**, and any smooth coordinate chart (U, x) on the manifold, short hand notation for 3.1.4.1, $g_{\alpha\beta} : U \to \mathbb{R}$. The **dimension** of a Riemannian manifold refers to the number of independent coordinates needed to specify a point on that manifold locally, in general denoted by n, a positive integer. As we already know, for spacetime geometry $n = 4$, as there are three independent spacial coordinates and one independent time coordinate. Unfortunately, it is rather complicated to express the infinitesimal geometry of a Riemannian manifolds for $n > 2$ as a single number at any point. To work with the **curvature** of Riemannian manifolds, Riemann introduced a way to define the curvature of those manifolds, this is known as the **Riemann curvature tensor R**, given by:

$$R^{\alpha}_{\beta\mu\nu} = \Gamma^{\alpha}_{\beta\mu,\nu} - \Gamma^{\alpha}_{\beta\nu,\mu} + \Gamma^{\alpha}_{\sigma\mu}\Gamma^{\sigma}_{\beta\nu} - \Gamma^{\alpha}_{\sigma\nu}\Gamma^{\sigma}_{\beta\mu} \tag{3.1.4.2}$$

where $\Gamma^{\alpha}_{\beta\mu,\nu} \equiv \frac{\partial}{\partial x^{\nu}}\Gamma^{\alpha}_{\beta\mu}$.

(*full derivation can be found at page 156-157 of A First Course in General Relativity [85]*). A locally inertial frame at a point $\mathcal{P}$, one can find that the component of **R** are given by the following (since $\Gamma^{\alpha}_{\mu\nu} = 0$ at $\mathcal{P}$):

$$R^{\alpha}_{\beta\mu\nu} = \frac{1}{2}g^{\alpha\sigma}\left(g_{\sigma\nu,\beta\mu} - g_{\sigma\mu,\beta\nu} + g_{\beta\mu,\sigma\nu} - g_{\beta\nu,\sigma\mu}\right) \tag{3.1.4.3}$$

where the Christoffel symbol was written in terms of the metric, see equation 3.1.1.5. Equation 3.1.4.3 leads to quite important results, starting with lowering the index α using the metric **g**;

$$R_{\alpha\beta\mu\nu} := g_{\alpha\lambda}R^{\lambda}_{\beta\mu\nu} = \frac{1}{2}\left(g_{\alpha\nu,\beta\mu} - g_{\alpha\mu,\beta\nu} + g_{\beta\mu,\alpha\nu} - g_{\beta\nu,\alpha\mu}\right) \tag{3.1.4.4}$$

From equation 3.1.4.4, one can verify the following identities:

$$R_{\alpha\beta\mu\nu} = -R_{\beta\alpha\mu\nu} = -R_{\alpha\beta\nu\mu} = R_{\mu\nu\alpha\beta} \tag{3.1.4.5}$$

$$R_{\alpha\beta\mu\nu} + R_{\alpha\nu\beta\mu} + R_{\alpha\mu\nu\beta} = 0 \tag{3.1.4.6}$$

Demonstrating equation 3.1.4.5,

$$R_{\alpha\beta\mu\nu} = \frac{1}{2}\left(g_{\alpha\nu,\beta\mu} - g_{\alpha\mu,\beta\nu} + g_{\beta\mu,\alpha\nu} - g_{\beta\nu,\alpha\mu}\right)$$

$$= \frac{1}{2}\left(g_{\beta\nu,\alpha\mu} - g_{\beta\mu,\alpha\nu} + g_{\alpha\mu,\beta\nu} - g_{\alpha\nu,\beta\mu}\right)$$

$$= -\frac{1}{2}\left(-g_{\beta\nu,\alpha\mu} + g_{\beta\mu,\alpha\nu} - g_{\alpha\mu,\beta\nu} + g_{\alpha\nu,\beta\mu}\right)$$

$$= -R_{\beta\alpha\mu\nu}$$

In the above equation we have simply swapped indices, α and β, and used the symmetric properties of the metric, i.e. $g_{\alpha\beta} = g_{\beta\alpha}$ and $g_{\alpha\beta,\mu\nu} = g_{\alpha\beta,\nu\mu}$ to then factor a global minus sign. Demonstrating the equation 3.1.4.6,

$$R_{\alpha\beta\mu\nu} + R_{\alpha\nu\beta\mu} + R_{\alpha\mu\nu\beta} = \frac{1}{2}(g_{\alpha\nu,\beta\mu} - g_{\alpha\mu,\beta\nu} + g_{\beta\mu,\alpha\nu} - g_{\beta\nu,\alpha\mu}$$

$$+ g_{\alpha\mu,\nu\beta} - g_{\alpha\beta,\nu\mu} + g_{\nu\beta,\alpha\mu} - g_{\nu\mu,\alpha\beta}$$

$$+ g_{\alpha\beta,\mu\nu} - g_{\alpha\nu,\mu\beta} + g_{\mu\nu,\alpha\beta} - g_{\mu\beta,\alpha\nu}) = \frac{1}{2} \times 0$$

$$R_{\alpha\beta\mu\nu} + R_{\alpha\nu\beta\mu} + R_{\alpha\mu\nu\beta} = 0$$

Hence, we can conclude that $R_{\alpha\beta\mu\nu}$ is anti-symmetric[85] on the first and second pair of indices, and symmetric[85] when swapping two pairs at the time. Furthermore, as the tensor equations 3.1.4.5 and 3.1.4.6 are true in one coordinate system, they must be true in all bases. Another important result is the following: *a manifold is flat if and only if* $R^{\alpha}_{\beta\mu\nu} = 0$ *[85].* For derivations see page 158-159 of [85].

3.1.5 Bianchi Identities, Ricci and Einstein Tensors

Consider the Riemann tensor at a local inertial coordinate, equation 3.1.4.4, now by differentiation the equation with respect to x^{λ}, one finds

$$R_{\alpha\beta\mu\nu,\lambda} = \frac{1}{2}\left(g_{\alpha\nu,\beta\mu\lambda} - g_{\alpha\mu,\beta\nu\lambda} + g_{\beta\mu,\alpha\nu\lambda} - g_{\beta\nu,\alpha\mu\lambda}\right) \tag{3.1.5.1}$$

From the above equation, the commutative property of partial derivatives and the symmetric property of the metric, we can find the following;

$$R_{\alpha\beta\mu\nu;\lambda} + R_{\alpha\beta\lambda\mu;\nu} + R_{\alpha\beta\nu\lambda;\mu} = 0 \tag{3.1.5.2}$$

The above set of tensor equations, is valid in any system. Equation 3.1.5.2 is know as the **Bianchi identities** [32, 85], which relate the covariant derivative of the Riemann curvature tensor to itself and to the metric tensor, where $R_{\alpha\beta\mu\nu;\lambda} \equiv R_{\alpha\beta\mu\nu,\lambda} - \Gamma^{\sigma}_{\lambda\alpha}R_{\sigma\beta\mu\nu} - \Gamma^{\sigma}_{\lambda\beta}R_{\alpha\sigma\mu\nu} - \Gamma^{\sigma}_{\lambda\mu}R_{\alpha\beta\sigma\nu} - \Gamma^{\sigma}_{\lambda\nu}R_{\alpha\beta\mu\sigma}$ (*see page 127 of [85]*).

For the purpose of this project we shall introduce the **Ricci tensor** [5, 85], in index notation denoted as $R_{\alpha\beta}$. The Ricci tensor is a second order tensor derived from derived from the Riemann curvature tensor, that encapsulates important information about the curvature of a Riemannian manifold. Consider $R^{\mu}_{\alpha\nu\beta}$, by contracting over the first and third indices we obtain the Ricci tensor, i.e.

$$R_{\alpha\beta} := R^{\mu}_{\alpha\mu\beta} = R_{\beta\alpha} \tag{3.1.5.3}$$

one contracts the Ricci tensor via the metric, to obtain another important quantity know as the **Ricci scalar**[6, 85],

$$R := g^{\mu\nu} R_{\mu\nu} \tag{3.1.5.4}$$

this is also obtained by contracting the Riemann curvature tensor twice via the metric, $R = g^{\mu\nu} g^{\alpha\beta} R_{\alpha\mu\beta\nu}$. This operation reduces the Ricci tensor from a second-order tensor to a scalar quantity, which represents the curvature of spacetime at a point. The Ricci scalar is a fundamental quantity in Einstein's field equations [66, 85, 89] of general relativity, which relate the curvature of spacetime to the distribution of matter and energy.

The **Einstein tensor** [64, 65, 85], denoted as $G_{\mu\nu}$, represents the left-hand side of Einstein's field equations, which describe the gravitational effects of matter and energy on the curvature of spacetime. The components of the Einstein tensor encode the gravitational field equations that govern the behavior of gravity according to general relativity. The Einstein tensor can be derived through the Ricci contraction to the Bianchi identities, the end result is the following:

$$G_{\mu\nu} \equiv R_{\mu\nu} - \frac{1}{2} g_{\mu\nu} R = G_{\nu\mu} \tag{3.1.5.5}$$

where $R_{\mu\nu}$ and R, are the Ricci tensor and the Ricci scalar respectively. It is important to know that the Einstein tensor is divergent free $\implies G_{\mu\nu;\nu} = 0$ (*look for derivation of Einstein tensor at page 163 of [85]*). Einstein field equations for GR are

$$G_{\mu\nu} = 8\pi G T_{\mu\nu} \tag{3.1.5.6}$$

where $T_{\mu\nu}$ is the stress-energy tensor, which describes the distribution and flow of matter and energy in spacetime. This is also divergent free, $T_{\mu\nu;\nu} \equiv 0$. And G is the gravitational constant. (*for more details on equation 3.1.5.6, see chapter 8 of [85]*).

3.2 Conserved Quantities Along the Geodesic

A conserved quantity[71, 99], in physics, is what we consider as a measurable property of a system that remains constant over time, even in a system that goes through various transformations or interactions. This quantities are fundamental to simplify calculations and to determine particle trajectories along a geodesic. In a closed system[1], quantities such as mass, energy and momentum (or angular momentum), remain constant in the absence of external influences. In Newtonian mechanics, for a particle, gravity is viewed as a force! Thus a particle's kinetic energy and momentum do not need to be conserved under its action. Hence, in GR one would not expect to find the components of $\vec{p}$ to be constant along the trajectory taken. Although there is an important exception, the geodesic equation can be written in therms of the components of $\vec{p}$:

$$m \frac{dp_{\alpha}}{d\tau} = \Gamma^{\mu}_{\alpha\beta} p^{\beta} p_{\mu} \tag{3.2.0.1}$$

[1] A closed system refers to a system that does not exchange matter with its surrounding.

Consider the right-hand side of equation 3.2.0.1, by expanding it we have:

$$\begin{aligned}\Gamma^{\mu}_{\alpha\beta}p^{\beta}p_{\mu} &= \frac{1}{2}g^{\mu\nu}\left(g_{\nu\alpha,\beta}+g_{\nu\beta,\alpha}-g_{\beta,\alpha,\nu}\right)p^{\beta}p_{\mu}\\ &= \frac{1}{2}\left(g_{\nu\alpha,\beta}+g_{\nu\beta,\alpha}-g_{\beta,\alpha,\nu}\right)g^{\mu\nu}p_{\mu}p^{\beta}\\ &= \frac{1}{2}\left(g_{\nu\alpha,\beta}+g_{\nu\beta,\alpha}-g_{\beta,\alpha,\nu}\right)p^{\nu}p^{\beta}\end{aligned}$$

Simplifying the above expression into:

$$\Gamma^{\mu}_{\alpha\beta}p^{\beta}p_{\mu} = \frac{1}{2}g_{\nu\beta,\alpha}p^{\nu}p^{\beta} \tag{3.2.0.2}$$

Here we have used the fact that the product $p^{\nu}p^{\beta}$ is symmetric in ν and α, while the terms $g_{\nu\alpha,\beta}$ and $g_{\beta\alpha,\nu}$, are anti-symmetric in ν and α, therefore they cancel, and we are left with the middle term. Now, one can collect the left-hand side of equation 3.2.0.1 with the right-hand side of equation 3.2.0.2, one can then write the geodesic equation as follows:

$$m\frac{dp_{\alpha}}{d\tau} = \frac{1}{2}g_{\nu\beta,\alpha}p^{\nu}p^{\beta} \tag{3.2.0.3}$$

Equation 3.2.0.3 provides the following important result: "if all the components $g_{\beta\nu}$ are independent of x^{α} for some fixed index α, then p_{α} is a constant along any particle's trajectory"(Bernard Schutz, 2022, p. 178)[85].

3.3 EinsteinPy

EinsteinPy[9, 56] is a Python[67] package designed to make it easier for users to work with concepts in GR. It provides tools for analyzing spacetime, computing orbits around massive objects like black holes, and understanding the behavior of particles and light in curved space. With EinsteinPy, users can perform calculations, visualize results, and explore the fascinating world of gravitational physics in a Pythonic environment.
Within EinsteinPy there is FANTASY[24] (Finally A Numerical Trajectory Algorithm both Straightforward and sYmplectic). FANTASY operates efficiently by simplifying the user input process. Rather than requiring the user to provide Christoffel symbols or metric derivatives, FANTASY only needs the metric and initial conditions for the geodesic. Through automatic differentiation, it accurately computes metric derivatives to machine precision, eliminating the need for manual input of conserved quantities. Furthermore, FANTASY can handle metrics that cannot be split into a (3 + 1) form, enabling integration in non-globally hyperbolic spacetime and Riemannian spaces. This versatility allows for the integration of geodesics in designer metrics with pathologies and statistical manifolds equipped with Fisher information metrics. The integration scheme employed by FANTASY is simplistic, ensuring bounded errors in conserved quantities. FANTASY comes with built-in second and fourth-order integration schemes and can be easily extended to higher-order (even) schemes for increased accuracy.

Chapter 4

Black Holes

This chapter covers all the material required for the chapter 5, where we will provide numerical solutions of particles trajectories in the proximity of black holes. Note we will not cover charged black holes (Reissner–Nordström[33, 47] and Kerr-Newman[104, 105]), as it goes beyond the scope of this project.

4.1 Background

Black holes[18, 46, 74] are theoretical objects predicted by GR. According to GR, when massive stars exhaust its nuclear fuel and it collapses under its own gravity, this can form a black hole. Where the gravitational pull is so strong that not even light can escape from it, hence the term "black hole". The boundary of no escape in a black hole is defined as the event horizon [80]. Initially, black holes were theoretical objects, but thanks to technological progress in astrophysics, the effects of black holes predicted from GR were observed, such that gravitational lensing, X-ray emission from the accretion disks, and gravitational waves. According to NASA [61], the first candidate for a black hole was first detected in 1964 (discovered by Jocelyn Bell Burnell [70]), when a sounding rocket detected a source of X-rays. In 1971, astronomers found that the X-rays where emitted by an unusual dark object orbited by a bright blue supergiant star, this suggested the presence of a black hole (Cygnus X-1 [76]). Today one of the most promising methods to detect black holes, is through the detection of gravitational waves [40, 91], these are ripples in spacetime caused by the acceleration of massive objects. Black holes in binary systems or during mergers can produce detectable gravitational waves. These propagate as waves outwards from their source at the speed of light. Advanced gravitational wave detectors like the Laser Interferometer Gravitational-Wave Observatory (LIGO) [2] and Virgo [3] have successfully detected gravitational waves from merging black holes, among these GW150914 [1]. This was the first-ever direct detection of gravitational waves, announced by the LIGO Scientific Collaboration and Virgo Collaboration in 2016. It resulted from the merger of two black holes with masses approximately $36M_\odot$ and $29M_\odot$ (where $M_\odot$ denotes the sun's mass which is $1.989 \times 10^{30} kg$), located about 1.3 billion light-years away.

4.1.1 Black Holes Structure

The no-hair theorem[1] [43, 49] (not proven) states that, a black hole, once it reaches a stable condition after it has formed, it will be characterised by three physical properties: mass, electric charge and angular momentum, these are all independent properties that can be detected by external observes.

[1] Proposed by John Wheeler in the 1960s [12],the no-hair theorem is still a conjecture that has not been proved.

If the conjecture is true, we would not be able to determine any differences between two black holes which share the same physical properties. These properties are important as they are visible from the outside of a black hole. For instance one can measure the angular momentum (the *spin*, denoted as a) through observation and measure the spin parameter of the black hole using frame dragging by the gravitational field, through the Lense-Thirring effect [78]. For the purposes of this project we are only going to analyse the structure of static and non-stat black holes (both uncharged) using the following diagrams:

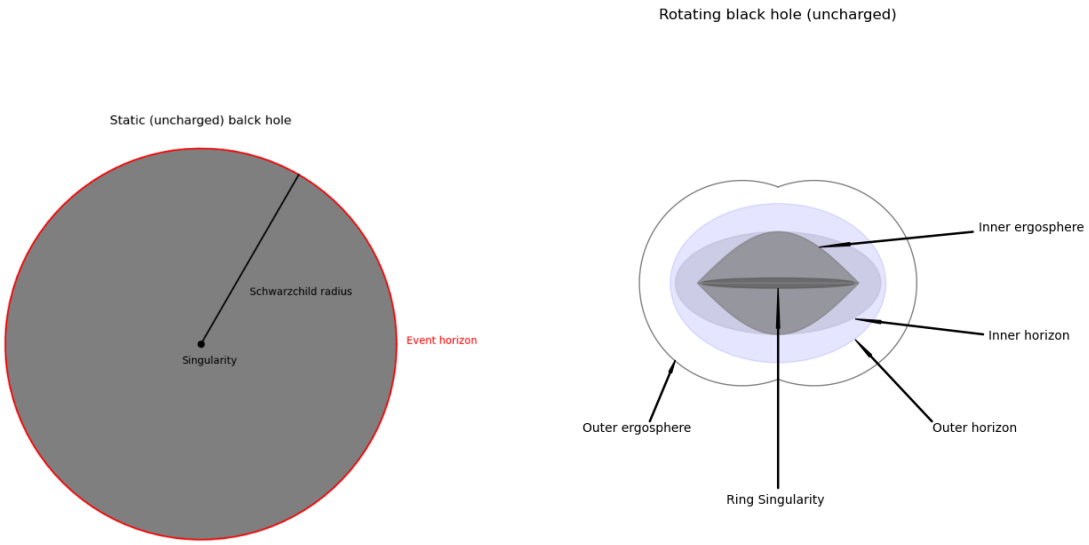

(a) Diagram 1 (b) Diagram 2

Figure 4.1: see link to code, for the above diagrams. Note these plots are just for illustration, they are not accurate.

We now want to analyse each component of the structure of two black holes, starting with the **static** black hole [98] (Schwarzschild black hole). For the static black hole the Schwarzschild radius defines the radius of the black hole, i.e. the distance between the boundary and the center of the black hole. At the center of a static black hole there is a singularity, where gravity is predicted to be so intense that spacetime itself would collapse, strictly speaking, in context of GR a singularity is a point in spacetime of infinite density. At the extremity of the Schwarzschild radius, it lies the event horizon (this is only valid for static black holes). A **non-static** or **rotating** black hole [45], known as a Kerr black hole, presents a dynamic and intricate spacetime landscape characterized by several distinct features. Surrounding the black hole is the outer *ergosphere* [42], a region where spacetime is dragged into rotation by the black hole's spin, forcing particles and light to co-rotate with it. Beyond the outer ergosphere lies the outer horizon, marking the point of no return for objects falling into the black hole. Deeper within, the inner ergosphere intensifies the rotational effects, allowing for the extraction of energy from the black hole's rotation. Within the inner horizon, an additional boundary, the inner horizon or Cauchy horizon, further complicates the spacetime structure, leading to phenomena such as closed timelike curves. At the heart of the black hole resides the *ring singularity* [81, 88], a spinning loop resulting from the rotation, which alters the spacetime geometry near the black hole. Together, these features of a rotating black hole create a complex gravitational environment that challenges our understanding of the fundamental nature of spacetime and gravity.

4.2 Black Hole Geometry

The geometry that describes the shape of a black hole can be written in terms of metrics. A static uncharged black hole described by the Schwarzschild metric [85, 96, 97] (this does not only describes the geometry of static black holes, but also celestial bodies, such us planets and stars). The geometry of a rotating uncharged black hole is given by the Kerr metric [10, 85, 90], in this section we will analyse the two metrics and their symmetries. Deriving them is beyond the scope of this project, for full derivation check Schwarzschild metric derivation [39] and Kerr metric derivation [90].

4.2.1 Schwarzschild Metric

The Schwarzschild metric is given by:

$$ds^2 = \left(1 - \frac{R_s}{r}\right) c^2 dt^2 - \left(1 - \frac{R_s}{r}\right)^{-1} dr^2 - r^2 d\Omega^2 \tag{4.2.1.1}$$

where:

$$d\Omega^2 = d\theta + \sin^2\theta d\phi^2 \tag{4.2.1.2}$$

$$R_s = \frac{2GM}{c^2} \tag{4.2.1.3}$$

R_s is the Schwarzschild radius, G is the gravitational constant, M is the mass of the central body and c is the speed of light in a vacuum. From this one can derive the null-like geodesic and the timelike geodesic, which can be used to determine particles motion around the central body, photons and massive particle respectively. More details on the symmetries of the Schwarzschild metric (very important, the Schwarzschild metric is characterised by spherical symmetry, this will lead to nice simplifications) can be found at the beginning of Chapter 5, where we will derive the null-like and timelike geodesics to then solve them using numerical computation.

4.2.2 Kerr Metric

The Kerr metric is an exact solution to the Einstein's field equation 3.1.5.6 of GR. Since these equations are extremely non-linear, they are very challenging to solve (due to the entity of this problem, in Chapter 5 we will not cover the derivation of any geodesics in a Kerr geometry, but rather provide and discuss plots of particle trajectories in the Kerr spacetime, these are obtained using the EinsteinPy package, all the codes will be provided through a shared link). Furthermore, as we have seen in section 4.1.1, the Kerr metric describes the spacetime around rotating uncharged axially symmetric[1] black holes with a quasi-spherical[2] event horizon (note the Kerr metric is NOT spherically symmetric, but instead this is rotationally symmetric about the momentum axis). The Kerr metric predicts dragging of inertial frame, which was recorded for the first time in 2011 by the Gravity Probe B experiment [36] (this is one of the many predictions from GR, that were found to be accurate).

The Kerr black hole (metric) is characterised by two parameters, its mass M and angular momentum J. One defines the dimensionless spin parameter $a := J/Mc$, where $a \in [0, 1]$. Hence we

[1] Axially symmetric refers to a property in which an object or system maintains the same appearance or behavior when rotated around its axis.

[2] Quasi-spherical refers to a shape or structure that is approximately spherical but may have some deviations from a perfect sphere.

can write the Kerr metric (written in terms Boyer–Lindquist coordinates [84]) as the following:

$$ds^2 = -\left(1 - \frac{R_s r}{\Sigma}\right) c^2 dt^2 + \frac{\Sigma}{\Delta} dr^2 + \Sigma d\theta + \left(r^2 + a^2 + \frac{R_s r a^2}{\Sigma} \sin^2\theta\right) \sin^2\theta d\phi^2 - \frac{2R_s r a \sin^2\theta}{\Sigma} c dt d\phi \tag{4.2.2.1}$$

where:

$$\Sigma = r^2 + a^2 \cos^2\theta \tag{4.2.2.2}$$

$$\Delta = r^2 - R_s r + a^2 \tag{4.2.2.3}$$

One can immediately see one of the major differences to the Schwarzschild metric 4.2.1.1, there is a cross-term, $g_{t\phi}$ (last term of equation 4.2.2.1), in the Kerr metric. Thus coupling between time and motion in the plane of rotation. If $a \to 0 \implies g_{t\phi} \to 0$, i.e. the black hole's angular momentum vanishes, and we get back to the Schwarzschild geometry. Another important feature, which is not illustrated in Figure 4.3 Diagram b, of the Kerr black hole is the innermost stable circular orbit (ISCO), the ISCO-radius is denoted as R_{ISCO} [82]. ISCO is the smallest marginal stable circular orbit which massive particles can orbit a rotating black hole. Depending on the spin parameter a of a black hole, one can determine the location of R_{ISCO}. In particular, R_{ISCO} marks the inner edge of the accretion disk [82] (also not included in the diagram). The accretion disk is a collection of material from the surrounding space can accrete onto the black hole's event horizon, forming a disk-shaped structure. The accretion disk is typically composed of gas, dust, and other stellar debris that is gradually drawn towards the black hole due to its immense gravitational pull. As the material spirals inward, it heats up and emits radiation across the electromagnetic spectrum, making accretion disks a prominent feature in the study of astrophysics. The equatorial ISCO in the Kerr metric depends on the sign of r_{ms}, negative sign (prograde orbit) and positive sign (retrograde orbit). The equation for r_{ms} is given by

$$r_{ms} = \frac{R_s}{2}\left(3 + Z_2 \pm \sqrt{(3 - Z_1)(3 + Z_1 + 2Z_2)}\right) \leq \frac{9}{2} R_s \tag{4.2.2.4}$$

where

$$Z_1 = 1 + \sqrt{1 - \chi^2}\left(\sqrt[3]{1 + \chi} + \sqrt[3]{1 - \chi}\right) \tag{4.2.2.5}$$

$$Z_2 = \sqrt{3\chi^2 + Z_1^2} \tag{4.2.2.6}$$

$$\chi = \frac{2a}{R_s} \tag{4.2.2.7}$$

As the rotaion of the black hole reaches its maximum i.e. $a = 1 \implies \chi \to 1$, progrede ISCO, the radius of the marginal bound orbit and the photo-sphere will shrink down to the event horizon. R_{ISCO} should not be confused with the Rochet limit [4], R_{ISCO} is related with theoretical test particles, not real object. Theoretically the location of R_{ISCO} is closer to the central object the location of Roche limit.

4.3 Event Horizon

We have already met and provided a basic definition in this chapter for the event horizon, as we can see from Figure 4.3, the event horizon for the static and rotating black holes are distinct. In this section we will delve into the concept of the event horizon, and what happens on the surface $r = R_s$.

4.3.1 Schwarzschild Horizon

The Schwarzschild horizon [8, 85] represents the boundary beyond which events cannot affect an outside observer. Any object or information that crosses the event horizon is inevitably drawn into the black hole's singularity and cannot escape. From an external observer's perspective, objects falling into the black hole appear to slow down and become increasingly red-shifted as they approach the event horizon, eventually freezing in time at the horizon's edge. The Schwarzschild horizon is characterized by its radius, $r = R_s$, which depends solely on the mass of the black hole. As the mass of the black hole increases, so does the radius of its event horizon, encompassing a larger region of spacetime from which no information can escape. Due to coordinate singularities, at the surface $r = R_s$ there is a **curvature singularity**, consider g_{rr} in equation 4.2.1.1, this component seems to diverge when $r = R_s$, this is quite misleading as we might think a particle falling in a static black hole would keep falling forever after crossing the event horizon. But we will shortly find out, this is not the case with a change in the coordinate system.

4.3.2 Schwarzschild metric in Kruskal-Szekeres Coordinates

When the problem of a particle "falling forever" was arised, the search for a change of coordinates began. This took a while and ended in 1960, where the coordinate system known as the Kruskal-Szekeres [59, 85] coordinates was formulated. One calls the new coordinates as u and v defined as follows:

$$\begin{aligned} u &= (r/R_s - 1)^{1/2} e^{r/2R_s} \cosh(t/R_s) \\ v &= (r/R_s - 1)^{1/2} e^{r/2R_s} \sinh(t/R_s) \end{aligned} \tag{4.3.2.1}$$

for $r > R_s$ and

$$\begin{aligned} u &= -(r/R_s - 1)^{1/2} e^{r/2R_s} \sinh(t/R_s) \\ v &= -(r/R_s - 1)^{1/2} e^{r/2R_s} \cosh(t/R_s) \end{aligned} \tag{4.3.2.2}$$

for $r < R_s$. (This coordinate transformation is singular at $r = R_s$, but this is a necessary to eliminate the coordinate singularity at the event horizon). Thus, by applying the new coordinate transformation to the Schwarzschild metric, one has the following:

$$ds^2 = \frac{4R_s^3}{r} e^{-r/R_s}(dv^2 - du^2) - r^2 d\Omega^2 \tag{4.3.2.3}$$

4.3.3 Kerr Horizon and Ergosphere

Unlike the non-rotating Schwarzschild black hole, the Kerr black hole exhibits a distorted, oblate shape due to its rotation. The Kerr horizon possesses two distinct regions: the outer horizon and the inner horizon. The outer horizon marks the boundary beyond which events cannot affect an outside observer and is similar to the Schwarzschild horizon. The Kerr horizon's shape and properties are determined by the black hole's mass and spin (angular momentum), influencing the dynamics of matter and radiation in its vicinity. For the Schwarzschild solution at the horizon $g_{tt} = 0$ and $g_{rr} \to \infty$, while in the Kerr solution the ergosphere occurs when $g_{tt} = 0$ and the horizon when $g_{rr} \to \infty$, i.e. when $\Delta = 0$:

$$r_{ergosphere} = \frac{R_s + \sqrt{R_s^2 - 4a^2 \cos^2\theta}}{2} \tag{4.3.3.1}$$

and

$$r_{horizon} = \frac{R_s + \sqrt{R_s^2 - 4a^2}}{2} \tag{4.3.3.2}$$

from the above we can deduce that the ergosphere lies outside the horizon except at the poles, where they are tangent to each other. Using EinsteinPy one can produce a 2D plot of the Kerr black hole for different values of a, the spin parameter.

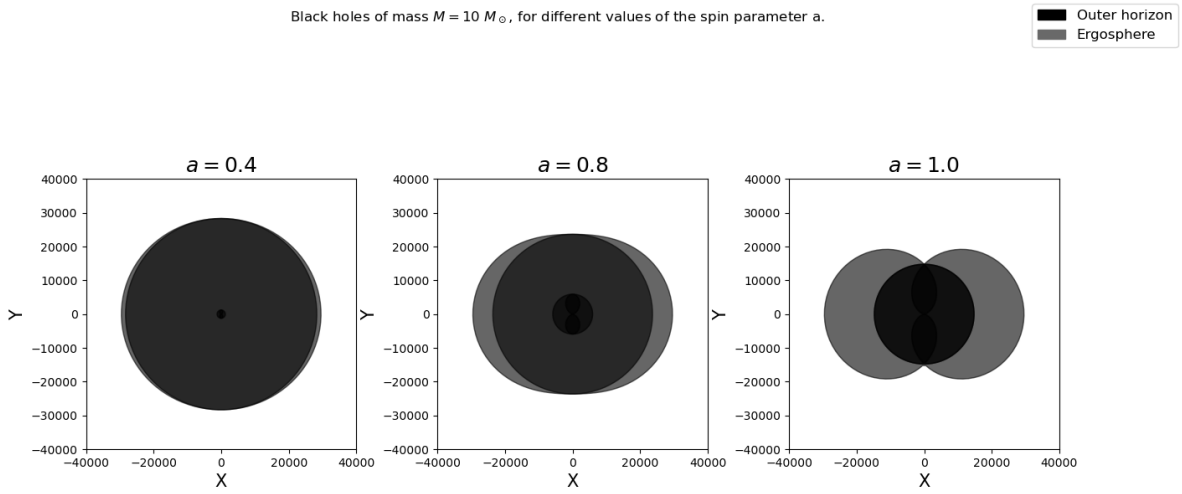

Figure 4.2: This plot illustrates how the ergosphere and other horizon change for different values of a and a fixed mass M. See link to code.

By using equations 4.3.3.1 and 4.3.3.2, one can produce a 3D plot of the Kerr black hole using matplotlib.pyplot in python.

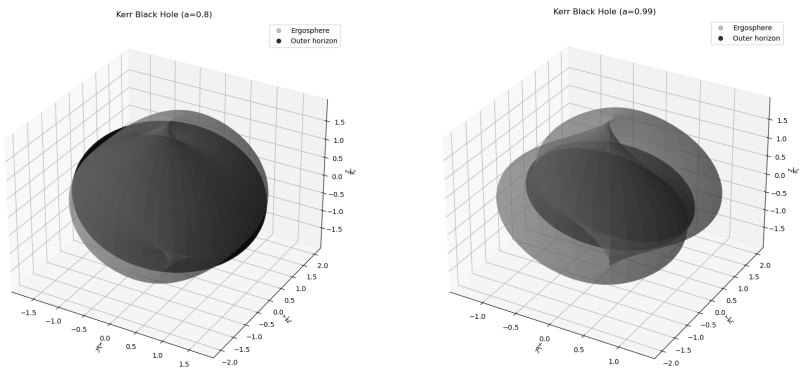

(a) 3D plot 1 (b) 3D plot 2

Figure 4.3: See Plotting, for the above 3D plots.

Chapter 5

Numerical Solutions to Particle's Trajectories

In this chapter we are going to solve the both Schwarzschild and Kerr geodesic using numerical integration. To begin, our plan is to use the Runge-Kutta 4 (RK4)[16, 106] and the python package einsteinpy to solve the Schwarzschild geodesic[37, 44, 85], subsequently we will plot all the set of data provided from each method. To end the chapter, we intend to solve the Kerr geodesic, and plot particles trajectories around a rotating (charged) black hole, due to the complexity of the problem we are going to fully rely on the package.

5.1 Schwarzschild Geodesic

To derive the Schwarzschild geodesic, one needs to find the Cristoffel symbols in the geodesic equation for each component of the Schwarzschild metric, we can start by recalling both the geodesic equation:

$$0 = \frac{d^2x^\sigma}{d\lambda^2} + \Gamma^\sigma_{\mu\nu}\frac{dx^\mu}{d\lambda}\frac{dx^\nu}{d\lambda} \tag{5.1.0.1}$$

(note instead of the proper time τ we use a parameter λ) for $x^\sigma = (ct, r, \theta, \phi)$ this leads to four different equations for each spacetime coordinate, and the Schwarzschild metric:

$$ds^2 = \left(1 - \frac{R_s}{r}\right)c^2dt^2 - \frac{1}{\left(1 - \frac{R_s}{r}\right)}dr^2 + r^2d\Omega^2 \tag{5.1.0.2}$$

where $d\Omega^2 = (d\theta^2 + \sin^2\theta d\phi^2)$. To simplify equation 5.1.0.2 one can take advantage of its spherical symmetries, i.e. the Schwarzschild metric is invariant under rotation in three dimensional space, in particular at $\theta = \pi/2$, therefore any geodesic moving in that plane will remain in the plain, the plane is totally geodesic[21]. The four different geodesics are:

Time equation, t

$$0 = \frac{d^2(ct)}{d\lambda^2} + \Gamma^t_{\mu\nu}\frac{dx^\mu}{d\lambda}\frac{dx^\nu}{d\lambda} \tag{5.1.0.3}$$

Radial equation, r

$$0 = \frac{d^2r}{d\lambda^2} + \Gamma^r_{\mu\nu}\frac{dx^\mu}{d\lambda}\frac{dx^\nu}{d\lambda} \tag{5.1.0.4}$$

Polar angle equation, θ

$$0 = \frac{d^2\theta}{d\lambda^2} + \Gamma^{\theta}_{\mu\nu}\frac{dx^\mu}{d\lambda}\frac{dx^\nu}{d\lambda} \tag{5.1.0.5}$$

Azimuthal angle equation, ϕ

$$0 = \frac{d^2\phi}{d\lambda^2} + \Gamma^{\phi}\mu\nu\frac{dx^\mu}{d\lambda}\frac{dx^\nu}{d\lambda} \tag{5.1.0.6}$$

Another important consequence of spherical symmetry, is that the Schwarzschild metric is **independent**[25] of the azimuthal angle ϕ and the time coordinate t, the surrounding spacetime looks the same in all directions (azimuthal symmetry[17]) and at all times (temporal symmetry[60]). This simplifies the analysis of the motion and gravitational effects in the Schwarzschild spacetime.

The next step is to determine all the Christoffel symbols for each of the above equations. As there are forty different Christoffel symbols for the Schwarzschild metric, must of the terms are zero, the calculation would be too lengthy, instead one can use the einsteinpy package and write a code on python, to compute all the non-zero Christoffel symbols, as it has been done (check link on symbols). By substituting the Christoffel symbols into equations 5.1.0.3, 5.1.0.4, 5.1.0.5 and 5.1.0.6, we obtain the following:

For the equation related to the time coordinate t, there are two non-zero Christoffel symbols;

$\Gamma^t_{rt} = \Gamma^t_{tr} = \frac{1}{2}\frac{R_s}{r(r-R_s)}$ by now substituting into equation 5.1.0.3 we obtain the following:

$$0 = \frac{d^2(ct)}{d\lambda^2} + \Gamma^t_{rt}\frac{dr}{d\lambda}\frac{d(ct))}{d\lambda} + \Gamma^t_{tr}\frac{d(ct)}{d\lambda}\frac{dr}{d\lambda}$$

$$= \frac{d^2(ct)}{d\lambda^2} + 2\Gamma^t_{rt}\frac{dr}{d\lambda}\frac{d(ct))}{d\lambda}$$

therefore:

$$0 = \frac{d^2(ct)}{d\lambda^2} + \frac{R_s}{r(r-R_s)}\frac{dr}{d\lambda}\frac{d(ct))}{d\lambda} \tag{5.1.0.7}$$

The above equation is particularly important as it leads to a constant of motion, i.e. $\frac{d(ct)}{d\lambda}(1 - R_s/r) = constant$, to very it one can take the derivative with respect to the parameter λ as follows:

$$\frac{d}{d\lambda}constant = \frac{d}{d\lambda}\left(\frac{d(ct)}{\lambda}\left(1 - \frac{R_s}{r}\right)\right)$$

$$= \frac{d^2(ct)}{d\lambda^2}\left(1 - \frac{R_s}{r}\right) + \frac{R_s}{r}\frac{dr}{d\lambda}\frac{d(ct))}{d\lambda} = 0$$

now divide by $r/(r - R_s)$ one gets back to our original equation 5.1.0.7, hence $\frac{d(ct)}{d\lambda}(1 - R_s/r)$ is conserved. In this case the conserved quantity is the total energy, let us denote the total energy of a massive particle as $\tilde{E} := p^0/m$, where m is the mass of the particle, and the energy of a photon as $E := p^0$, where p^0 is the first component of the four-momentum $\vec{p}$.

Photon

$$E = \frac{d(ct)}{d\lambda}\left(1 - \frac{R_s}{r}\right) \implies \frac{d(ct)}{d\lambda} = E\left(1 - \frac{R_s}{r}\right)^{-1} \tag{5.1.0.8}$$

Massive particle

$$\tilde{E} = \frac{d(ct)}{d\tau}\left(1 - \frac{R_s}{r}\right) \implies \frac{d(ct)}{d\tau} = \tilde{E}\left(1 - \frac{R_s}{r}\right)^{-1} \tag{5.1.0.9}$$

Here, for a massive particle, we replace the parameter λ, with the proper time τ. Note, for both equations 5.1.0.8 and 5.1.0.9 if we take the limit of $r \to \infty$ one gets back to the four-momentum in SR. If we repeat a similar process for the radial coordinate equation, which does not lead to any conserved quantities, one can find that there are four non-zero Christoffel symbols $\Gamma^r_{tt} = -R_s(R_s/2r - 1/2)/r^2$, $\Gamma^r_{rr} = R_s(R_s/2r - 1/2)/(r^2(-R_s/r + 1)^2)$, $\Gamma^r_{\theta\theta} = 2r(R_s/(2r) - 1/2)$ and $\Gamma^r_{\phi\phi} = 2r(R_s/2r - 1/2)\sin^2\theta$, thus the radial equation reduces to:

$$0 = \frac{d^2r}{d\lambda^2} + \frac{1}{2}\left[\frac{R_s(r - R_s)}{r^3}\left(\frac{d(ct)}{d\lambda}\right)^2 + \frac{R_s}{r(R_s - r)}\left(\frac{dr}{d\lambda}\right)^2\right] + (R_s - r)\left(\frac{d\phi}{d\lambda}\right)^2 \tag{5.1.0.10}$$

The polar angle equation, regarding the angle θ, will vanish as $\theta = \pi/2$ is constant. But another important geodesic is given by the azimuthal angle equation (equation 5.1.0.6), which will lead to another important constant of motion. There are two non-zero Christoffel symbols:

$\Gamma^\phi_{\phi r} = \frac{1}{r}$ and $\Gamma^\phi_{\theta\phi} = \cot\theta$

After applying the above Christoffel symbols to equation 5.1.0.6, and some algebraic manipulations, we have

$$0 = \frac{d^2\phi}{d\lambda^2} + \frac{2}{r}\frac{dr}{d\lambda}\frac{d\phi}{d\lambda} \tag{5.1.0.11}$$

As mentioned above, this equation leads to another constant of motion, which is given by $r^2 d\phi/d\lambda$, in particular this conserved quantity corresponds to the angular momentum for particles. Let the angular momentum for massive particles be $\tilde{J} = p^\phi/m$, where m is the mass of the particle and p^ϕ is the angular momentum between two bodies (in particular, it corresponds to the 4^{th} of the four-momentum), and for photons $J = p^\phi$. As before:

Photon

$$J = r^2\frac{d\phi}{d\lambda} \implies \frac{d\phi}{d\lambda} = \frac{J}{r^2} \tag{5.1.0.12}$$

Massive particle

$$\tilde{J} = r^2\frac{d\phi}{d\tau} \implies \frac{d\phi}{d\tau} = \frac{\tilde{J}}{r^2} \tag{5.1.0.13}$$

Having found the constants of motion, we can now proceed to determine the magnitude square of the vector $d/d\lambda$:

$$\left|\left|\frac{d}{d\lambda}\right|\right|^2 = \frac{d}{d\lambda}\cdot\frac{d}{d\lambda}$$

$$= \left(\frac{dx^\mu}{d\lambda}\frac{\partial}{\partial x^\mu}\right)\cdot\left(\frac{dx^\nu}{d\lambda}\frac{\partial}{\partial x^\nu}\right) = \frac{dx^\mu}{d\lambda}\frac{dx^\nu}{d\lambda}\left(\frac{\partial}{\partial x^\mu}\cdot\frac{\partial}{\partial x^\nu}\right)$$

$$= \frac{dx^\mu}{d\lambda}\frac{dx^\nu}{d\lambda}g_{\mu\nu}$$

$$= \left(\frac{d(ct)}{d\lambda}\right)^2 g_{tt} + \left(\frac{dr}{d\lambda}\right)^2 g_{rr} + \left(\frac{d\theta}{d\lambda}\right)^2 g_{\theta\theta} + \left(\frac{d\phi}{d\lambda}\right)^2 g_{\phi\phi}$$

$$= \left(\frac{d(ct)}{d\lambda}\right)^2\left(1-\frac{R_s}{r}\right) - \left(\frac{dr}{d\lambda}\right)^2\left(1-\frac{R_s}{r}\right)^{-1} - \left(\frac{d\phi}{d\lambda}\right)^2 r^2\sin^2\theta$$

therefore

$$\left|\left|\frac{d}{d\lambda}\right|\right|^2 = \left(\frac{d(ct)}{d\lambda}\right)^2\left(1-\frac{R_s}{r}\right) - \left(\frac{dr}{d\lambda}\right)^2\left(1-\frac{R_s}{r}\right)^{-1} - \left(\frac{d\phi}{d\lambda}\right)^2 r^2 \tag{5.1.0.14}$$

depending on the value of $\|d/d\lambda\|^2$, we have the following:

- $\left|\left|\frac{d}{d\lambda}\right|\right|^2 = 0$ for light-like geodesic (photons)
- $\left|\left|\frac{d}{d\lambda}\right|\right|^2 = \left|\left|\frac{d}{d\tau}\right|\right|^2 = c^2 > 0$ for time-like geodesic (massive particles)

Rearranging equation 5.1.0.14, and substituting the conserved quantities, we have the following equation of motions:

Photon

$$\left(\frac{dr}{d\lambda}\right)^2 = E^2 - \left(1-\frac{R_s}{r}\right)\frac{J^2}{r^2} \tag{5.1.0.15}$$

Massive particle

$$\left(\frac{dr}{d\tau}\right)^2 = \tilde{E}^2 - \left(1-\frac{R_s}{r}\right)\left(c^2 + \frac{\tilde{J}^2}{r^2}\right) \tag{5.1.0.16}$$

One can further simplify each of the above ordinary differential equations (ODEs), by multiplying both sides by the angular momentum, to eliminate the parameter λ and the proper time τ, so that we obtain two ODEs that only depend on two coordinates, namely r and ϕ.

Photon

$$\left(\frac{d\lambda}{d\phi}\frac{dr}{d\lambda}\right)^2 = E^2 - \left(1 - \frac{R_s}{r}\right)\frac{J^2}{r^2} \times \left(\frac{r^2}{J}\right)^2$$

$$\left(\frac{dr}{d\phi}\right)^2 = E^2\left(\frac{r^2}{J}\right)^2 - \left(r^2 - R_s r\right)$$

thus the equation of motion for photon in a Schwarzschild geodesic is modelled by,

$$\frac{dr}{d\phi} = \pm\sqrt{E^2\left(\frac{r^2}{J}\right)^2 - (r^2 - R_s r)} \tag{5.1.0.17}$$

Similarly, if we apply the same process for massive particles, we have the following equation of motion,

$$\frac{dr}{d\phi} = \pm\frac{r^2}{\tilde{J}}\sqrt{\tilde{E}^2 - \left(1 - \frac{R_s}{r}\right)\left(c^2 + \frac{\tilde{J}^2}{r^2}\right)} \tag{5.1.0.18}$$

For both cases, mass and massless particles, the convention of the minus or plus sign depends whether the particle is falling inwards or outwards the central mass (black hole). Let us define the effective potentials of each ODEs (5.1.0.15, 5.1.0.16) as $V^2(r)$ and $\tilde{V}^2(r)$, where:

$$\text{photon:} \quad V^2(r) = \left(1 - \frac{R_s}{r}\right)\frac{J^2}{r^2} \tag{5.1.0.19}$$

$$\text{massive particle:} \quad \tilde{V}^2(r) = \left(1 - \frac{R_s}{r}\right)\left(c^2 + \frac{\tilde{J}^2}{r^2}\right) \tag{5.1.0.20}$$

Now we have all the necessary tools do plot photons and massive particles trajectories, by solving the ODEs 5.1.0.17 and 5.1.0.18, and plotting the results in a xy plane.

5.1.1 Using Runge Kutta 4 (RK4)

The Runge-Kutta (RK) method is a widely used numerical technique for solving ordinary differential equations (ODEs). Specifically, the Runge-Kutta 4th order (RK4)[16, 106] method is one of the most popular and accurate methods for solving initial value problems (IVPs). The RK4 method is based on the idea of advancing the solution of an ODE by computing a weighted average of several intermediate slopes within each time step. By using higher-order polynomial approximations, RK4 achieves greater accuracy compared to simpler methods like Euler's method [27].

Algorithm breakdown

Given an initial value problem $\frac{dy}{dt} = f(t, y)$ with initial condition $y(t_0) = y_0$, then the algorithm undergoes the following procedure:

- Set the initial time $t = t_0$ and the initial solution $y = y_0$
- Specify the step size h and the final integration time t_{end}

At each step t_n:

- compute the slope k_1 at t_n, i.e $k_1 = f(t_n, y_n)$
- compute the slope k_2 at $t_n + \frac{h}{2}$ using $y_n + \frac{h}{2}k_1$, i.e. $k_2 = f\left(t_n + \frac{h}{2}, y_n + \frac{h}{2}k_1\right)$
- compute the slope k_3 at $t_n + \frac{h}{2}$ using $y_n + \frac{h}{2}k_2$, i.e. $k_3 = f\left(t_n + \frac{h}{2}, y_n + \frac{h}{2}k_2\right)$
- compute the slope k_4 at $t_n + h$ using $y_n + hk_3$, i.e. $k_4 = f(t_n + h, y_n + hk_3)$
- hence the updated solution:
  $y_{n+1} = y_n + \frac{h}{6}(k_1 + 2k_2 + 2k_3 + k_4)$
- update the time: $t_{n+1} = t_n + h$
- termination: repeat the iterative process until $t_n \geq t_{end}$ or the desired number of iterations reached.

In this section, all the results are obtained through solving the equations of motions using RK4 method, given some specific initial conditions, and values for angular momentum and total energy. But before proceeding, it would be useful to see plots of the effective potentials and their physical interpretations, starting with:

photons, for the below plot see link to plot.

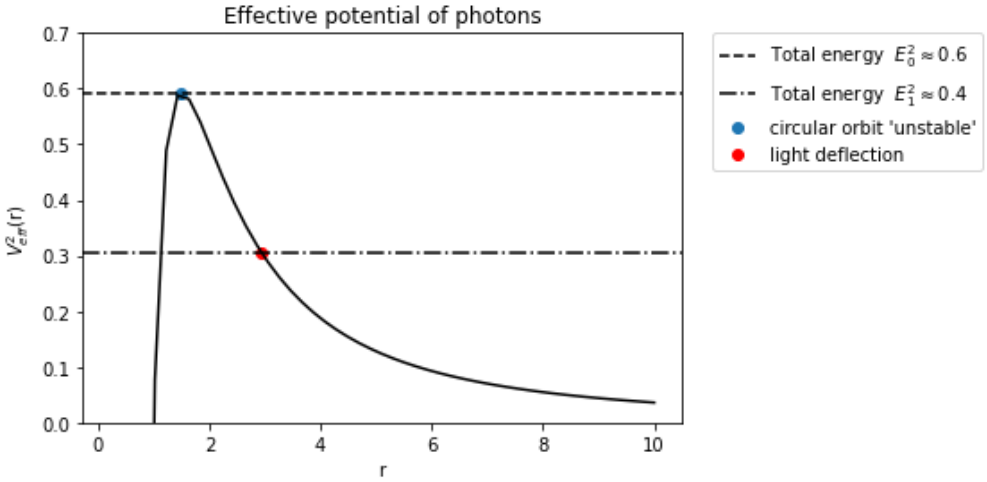

Figure 5.1: This is a plot of the effective potential[62] for a photon, for a specific angular momentum, in particular $J = 2$ in the code, as a function of r.

When the total energy is at the maximum of the curve, i.e. $E_0^2 \approx 0.6$, light rays will orbit the singularity in a "unstable" circular orbit[73], at a constant radial distance of $r = \frac{3}{2}R_s$. Unstable means, any small perturbation could cause photons to either fall in the singularity or escape to infinity. Below we have a plot of the solution to the ODE 5.1.0.17, for the total energy E_0^2 (for plot 5.2 see link to plot).

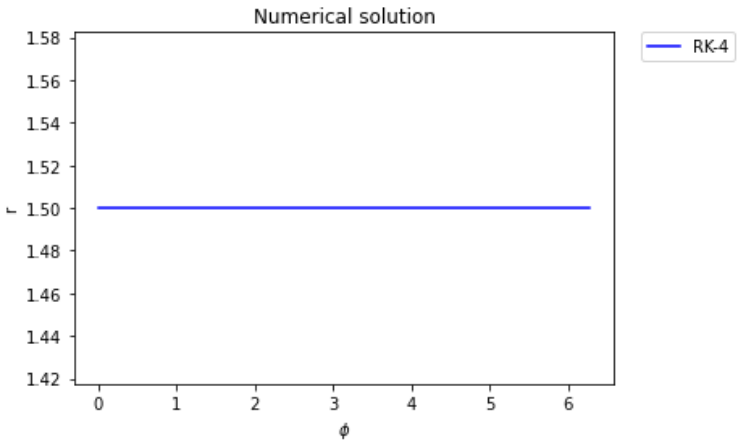

Figure 5.2: Plot shows a numerical solution, to the ODE 5.1.0.17.

As we can see from the above plot, when we solve for r given that the total energy is $E^2 = E_0^2$, for an initial value of $r_0 = \frac{3}{2}R_s$, and for initial and ending values of $\phi_0 = 0$ and $\phi_{end} = 2\pi$, the value of r stays constant. Now we can plot the values of r and ϕ in an xy plane obtaining the following plot (use the same link available from the previous plot 5.2);

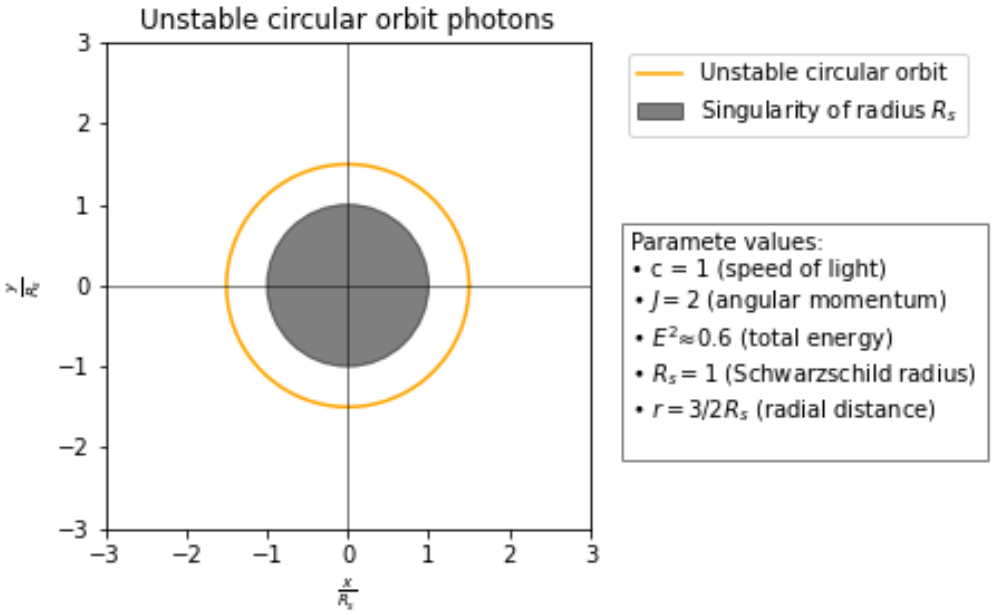

Figure 5.3: The region $r = \frac{3}{2}R_s$ is known as the photo-sphere[72, 50] of a non-rotating black hole. Within this radius, the gravitational pull of the black hole is strong enough to bend light around it, allowing for these unstable orbits.

The next step is solve the ODE 5.1.0.17 for the other value of the total energy in plot 5.1, if we then set the total energy $E^2 = E_1^2$, and for specific initial conditions of r and ϕ, we obtain the following plots

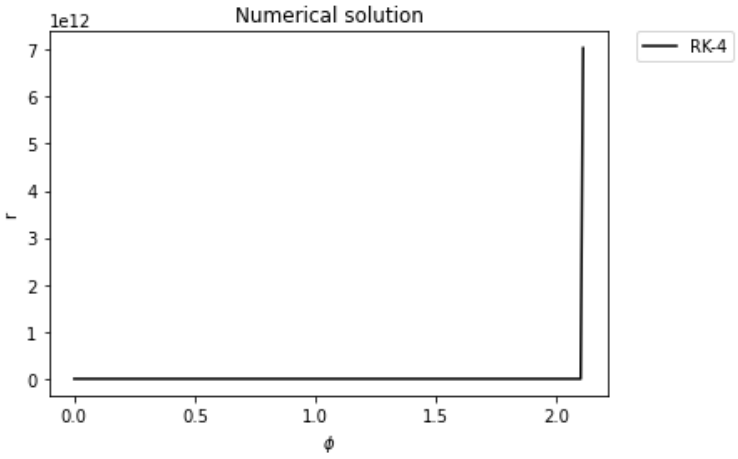

Figure 5.4: This plots shows a half of a parabolic solution to determine r as a function of ϕ. Unfortunately the RK4 method is quite limited, as we will also see for future plots, for example the algorithm will stop when the gradient is zero, or in this case it does not provide the full information required to understand the functions behaviour. Initial values: $r \approx 2.93$ and $\phi = 0$.

Since we do not have a full picture of what is happening, one can extrapolate what the rest of the values would look like on the negative ϕ-axis, as a result;

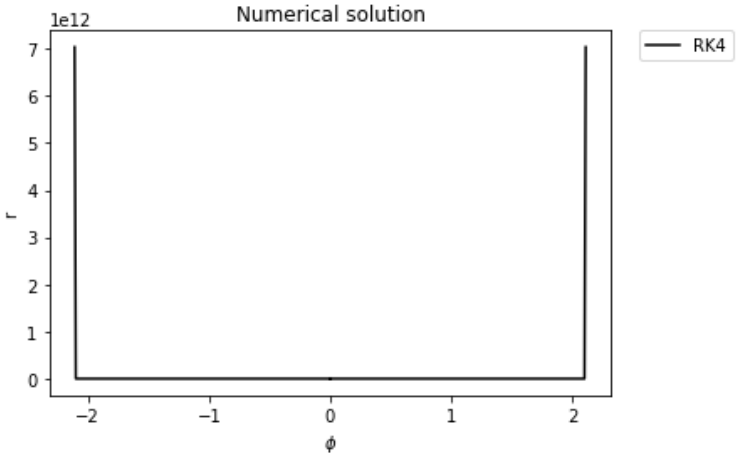

Figure 5.5: Mathematically this could be incorrect, if we consider the existence and uniqueness of an ODE (this is beyond our interest). But this is what we expect physically, as the photons are not being captured given all the conditions applied, instead the trajectory will be slightly bend by the singularity, this has a parabolic behaviour. The same initial conditions apply here.

One can now use the data provided in Figure 5.5, to plot the photons trajectory in a xy-plane

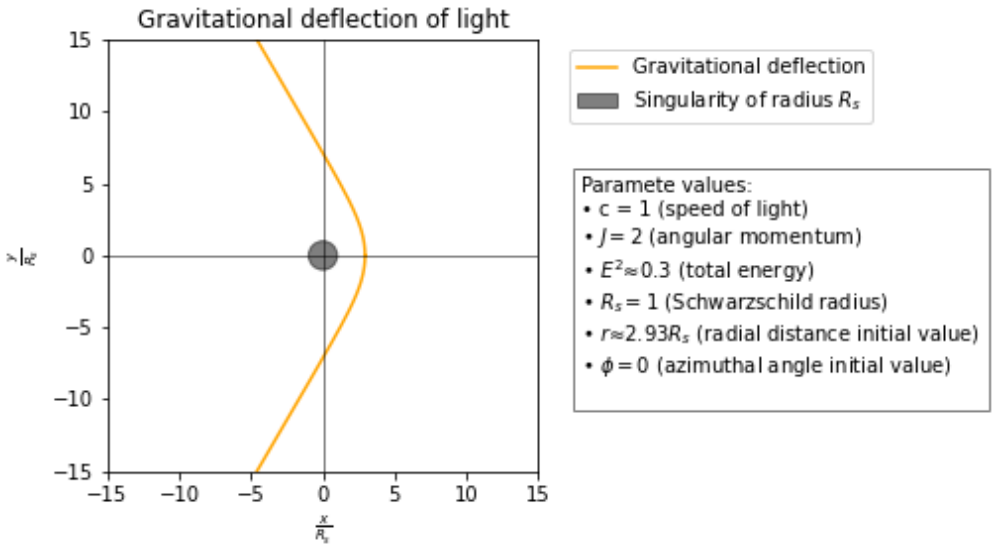

Figure 5.6: This plots shows gravitational deflection of light near a singularity, this concept is very important as demonstrated the accuracy of the theory of GR in an experiment in 1919.

Light deflection experiment[31, 101]:
The 1919 experiment to confirm Einstein's General Theory of Relativity was conducted by Sir Arthur Eddington[20] during a total solar eclipse. The theory predicted that the gravitational field of the Sun would cause the light from stars passing near the Sun to be bent due to the curvature of spacetime. Eddington observed the positions of stars during the eclipse and compared them to their positions when the Sun was not in the vicinity. He found that the positions of the stars appeared shifted due to the gravitational bending of light around the Sun, confirming one of the key predictions of Einstein's theory. This experimental verification provided strong evidence for the validity of General Relativity and contributed significantly to its acceptance within the scientific community. (For the above plots see link to light obits)

Massive Particles

Until now, we have been focusing on massless particles, i.e. photon, but it is time for us to move on to what is more relevant for the purposes of this project, massive particles! We have seen that the equations of motions for photons and massive particles are quite similar, but those small differences play a very important role. Before presenting the numerical solution plots, we shall analyse, as before for photons, the graph of effective potential against r.

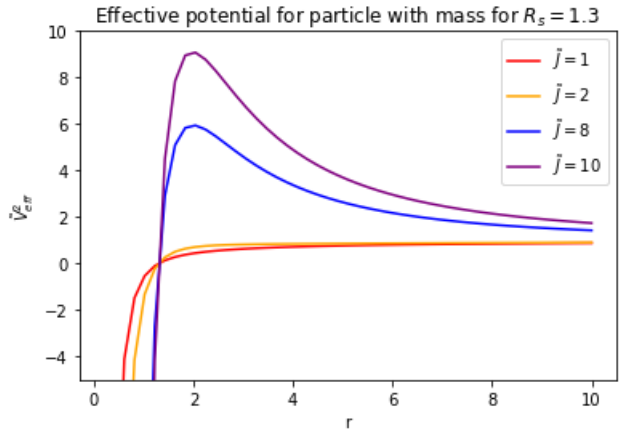

Figure 5.7: This plot shows how the effective potential changes according to the value of the angular momentum $\tilde{J}$.

Let us choose of the values of the angular momentum from the above picture, so that we can work with that specific angular momentum.

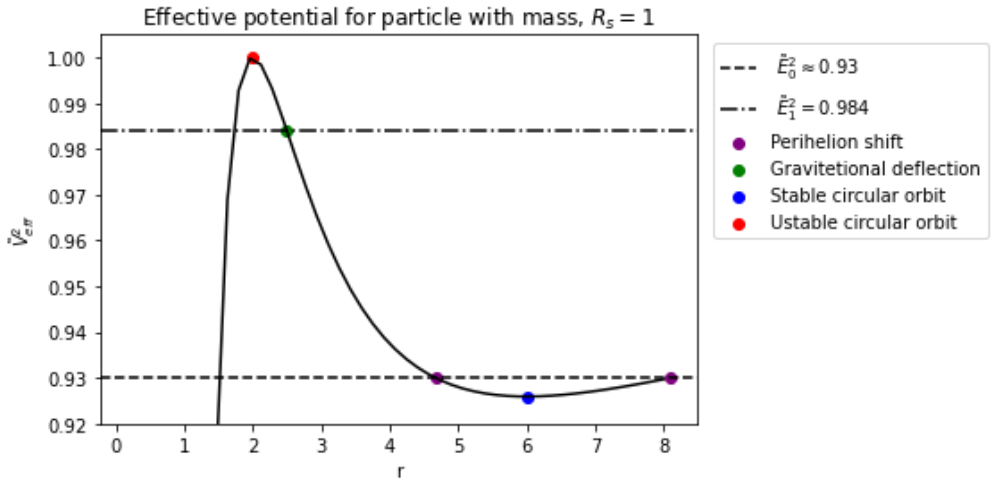

Figure 5.8: Effective potential[62] for a particle
[see link for the plot]

One can start with the simplest type of orbit, **circular orbits**. To derive the two possible circular orbits it is not necessarily required to solve ODE 5.1.0.16, instead one can set r as a constant to be determined, if $r = constant \implies dr/d\tau = 0$. Therefore the left-hand side of equation 5.1.0.16. By

differentiating both sides with respect to r

$$\frac{d}{dr}0 = \frac{d}{dr}\left[\tilde{E}^2 - \left(1 - \frac{R_s}{r}\right)\left(c^2 + \frac{\tilde{J}^2}{r^2}\right)\right]$$

$$0 = \frac{R_s}{r^2}\left(c^2 + \frac{\tilde{J}^2}{r^2}\right) - 2\left(1 - \frac{R_s}{r}\right)\frac{\tilde{J}^2}{r^3} = R_s c^2 r^2 + 3R_s\tilde{J}^2 - 2r\tilde{J}^2$$

Solve for r using the quadratic formula,

$$r = \frac{\tilde{J}^2 \pm \sqrt{\tilde{J}^4 - 3R_s^2 c^2 \tilde{J}^2}}{R_s c^2} \tag{5.1.1.1}$$

Therefore when r is constant we have two possible values. The negative signs will provide a smaller value of r, i.e. the circular orbit will be closer to the singularity, thus the orbit is unstable. For the positive sign, the orbit traced from the particle is on the outer region, this is the stable circular orbit. One can plot both orbits for the same period of 2π, leading to the following plot for stable and unstable circular orbits[48] (to see the code used to produce the plot below, see link to circular orbits and effective potentials).

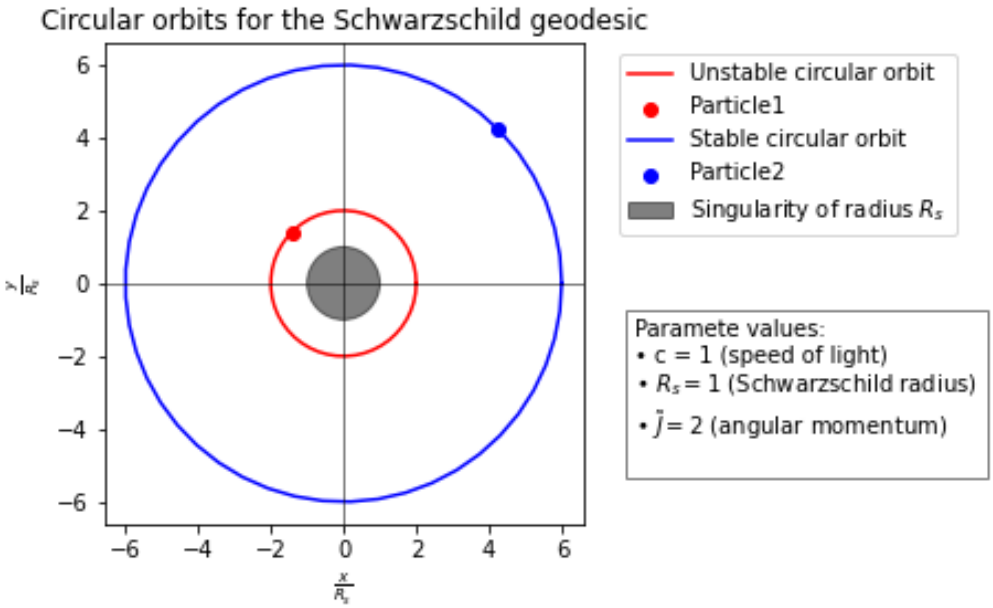

Figure 5.9: The inner circle represents the unstable circular orbit, outer circle the stable circular orbit.

The next part will be on the perihelion shift[92, 94]. The perihelion shift is a phenomenon in orbital mechanics that describes the gradual rotation of the point of closest approach (perihelion) of a celestial body's orbit. In the context of GR, it specifically refers to the observed deviation from the predicted position of the perihelion of a planet's orbit around the Sun. According to Newtonian mechanics[23], planetary orbits should remain fixed in space over time. However, in GR, the presence

of massive objects like the Sun causes spacetime to curve, affecting the motion of nearby objects. This curvature leads to a small but measurable shift in the perihelion of a planet's orbit over time, which is known as the perihelion shift. The perihelion shift has been observed and confirmed through astronomical observations, providing empirical evidence for the validity of GR. Solving equation 5.1.0.16, for a value of total energy $\tilde{E}^2 \approx 0.93$ (look at the dotted line in plot5.1.0.20), and for an initial value of $r_0 = 4.673R_s$, we get the following solution (see all codes for the perihelion shift in link to perihelion shift):

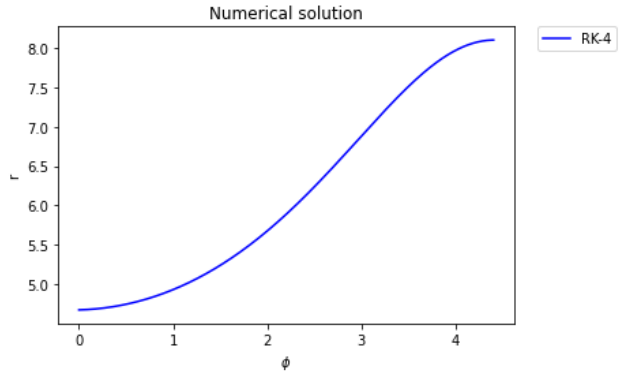

Figure 5.10: Due to reaching the gradient to be equal to zero, the RK4 algorithm stops, physically we know that the curve is meant to continue oscillating between two values of r.

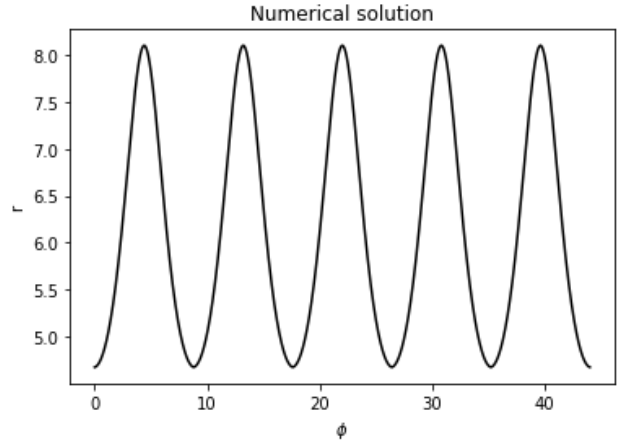

Figure 5.11: Extrapolated solution given the values of the previous plot5.10.

As we have seen with photons, what happens when unstable circular orbits are perturbed, is that photons/massive particles will either be shot to infinity or fall in the singularity. When there is a perturbation in the stable circular orbit (massive particles only), then the value of the radial distance will fluctuate between two values, a maximum and minimum distance. This is what the next few plots represent.

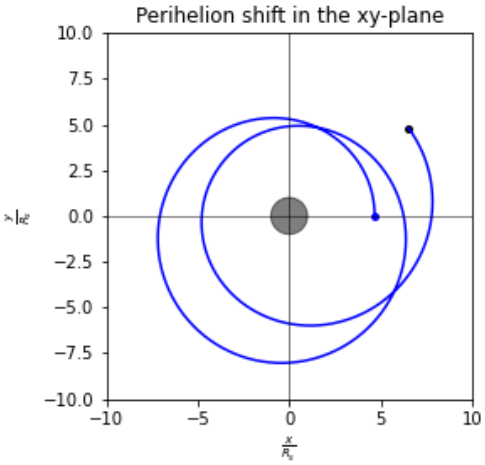

(a) Plot 1

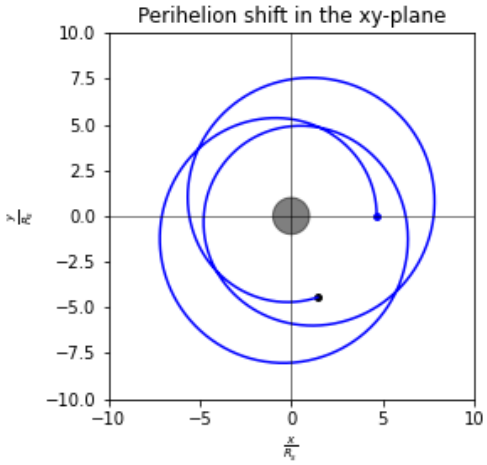

(b) Plot 2

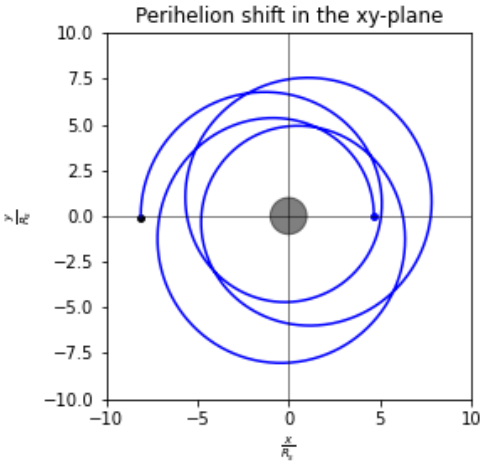

(c) Plot 3

Figure 5.12: The blue dot, in each plot is the initial position of the particle, and the black dot is the particle tracing the trajectory.

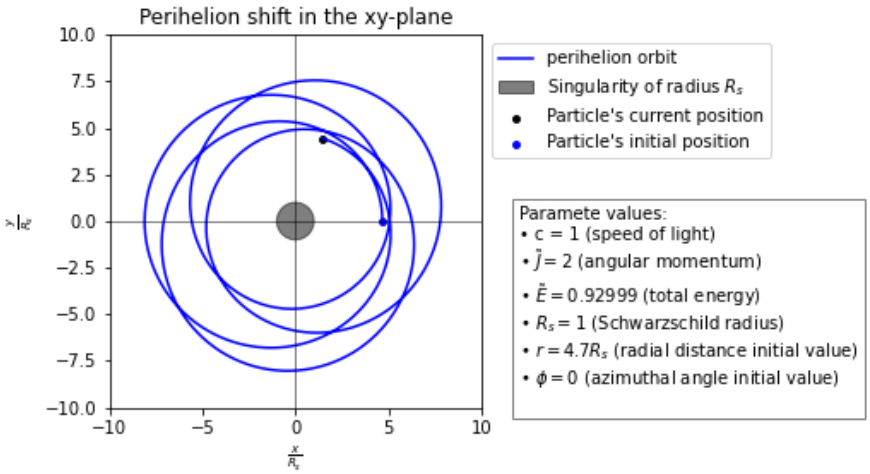

Figure 5.13: The last and final plot, for the perihelion shift, is next to the legend, and a text box with all the input values in the code. As we can notice the perihelion shift of the particle's trajectory is rather large for this particular plot, this is because the initial position of the particle is in the proximity of the singularity, hence the larger shift is recorded. A perfect example is valid for the orbit of Mercury around the Sun, the shift is larger and more noticeable compare to the other planets in our solar system, as Mercury is the closest planet to the Sun.

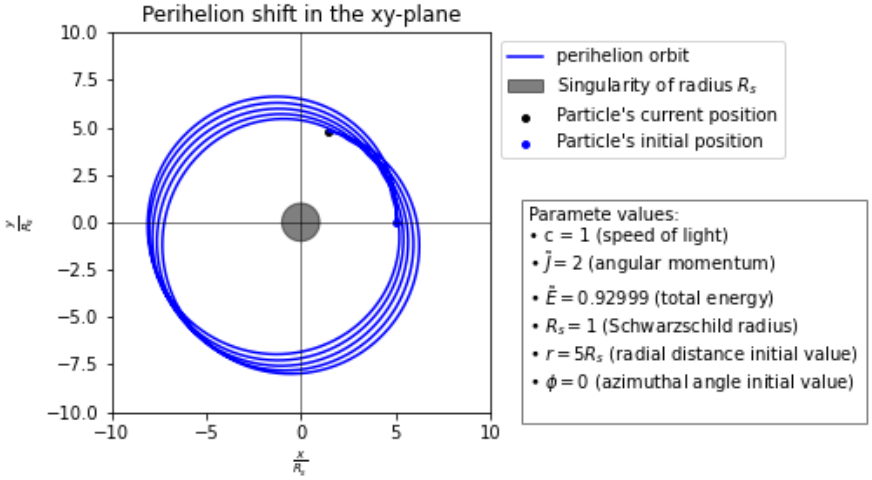

Figure 5.14: This is an example of what happens to the shift as we change our initial condition to $r_0 = 5R_s$ from the original code, the perihelion shift has reduced drastically as the particle is now further away from the singularity compared to the previous plot.

Having provided solutions for elliptical shifted orbits, let us now analyse what happens for perturbations in particular when the massive particle has enough energy to escape the singularity. From plot 5.1.0.20, consider when the total energy is $\tilde{E}^2 = 0.984$, and the chosen initial value for $r_0 = 2.4R_s$, then the numerical solution to equation 5.1.0.16, is shown in the plot below: Plotting

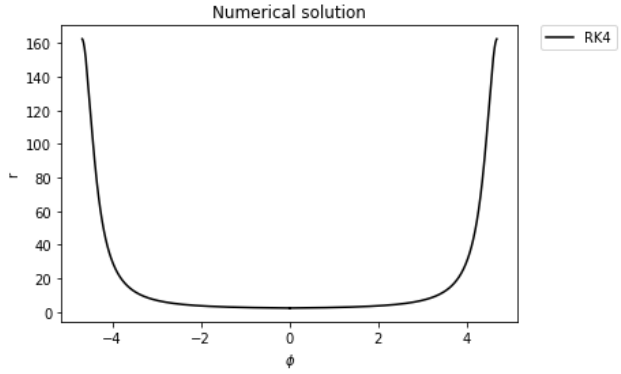

Figure 5.15: From the numerical solution, one can already observe that the particle is captured from the singularity, to the be repelled again.

the above data in a xy-plane:

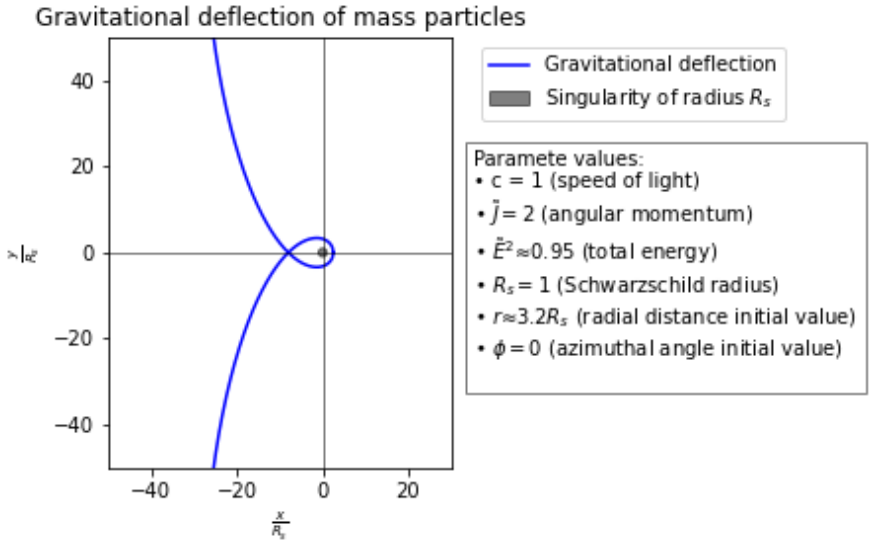

Figure 5.16: This plot shows a parabolic orbit[69] of a particle, where the particle is initially captured by the center of mass, but then repelled away.

5.1.2 Using EinsteinPy

At the end of Chapter 3 we have introduced EinsteinPy [9, 56] a Python library that can be used to solve the Schwarzschild and Kerr geodesics. The main purpose of using the RK4 method to solve the Schwarzschild geodesic was to provide a deeper understanding of particle trajectories, and to use it as a benchmark for the EinsteinPy package. It is important to note that EinsteinPy has its own plotting libraries, to be able to compare some of the plots produced with the package

to RK4 plots, it is essential to use the same plotting libraries, hence using the package to solve the Schwarzschild geodesic, for different parameters, and then plot the solutions independently (using the standard matplotlib.pyplot). As before, we will see plots of both massive particles and photons around the Schwarzschild black hole, the package has two inbuilt functions that allows to be solved for timelike (importing Timelike from EinsteinPy) and lightlike (importing Nulllike from EinsteinPy) geodesics. The package, by default, sets all the physical constants equal to one, i.e. $G = M = c = 1 \implies R_s = 2$, (where G is the gravitational constant, M is the mass of the central object and c is the speed of light in a vacuum) for the RK4 method we had $R_s = 1$, so to match the solutions previously obtained, one has to double the values of the initial conditions previously used, e.g. if the initial condition for the radial coordinate was $r_0 = 4.7R_s$, now we have that $r_0 = 9.4R_s$.

Timelike geodesic

As mentioned before, EinsteinPy has its own plotting libraries, starting with the perihelion shift. Here, there is a plot obtained with the those libraries:

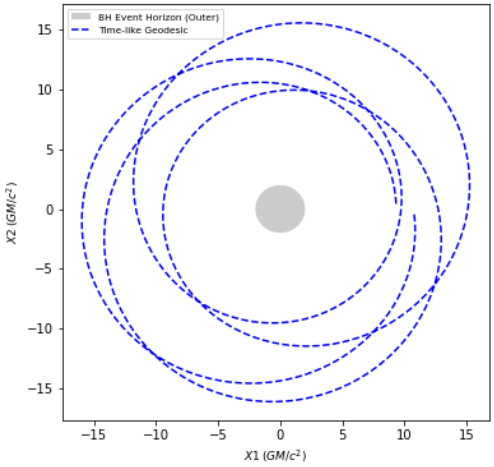

(a) This is a plot generated with the plotting libraries of EinsteinPy. Here, are: the initial values are, initial position = $(9.346, \pi/2, 0) \equiv (r, \theta, \phi)$ and momentum = $(0, 0, 4) \equiv (p^r, p^\theta, p^\phi)$.

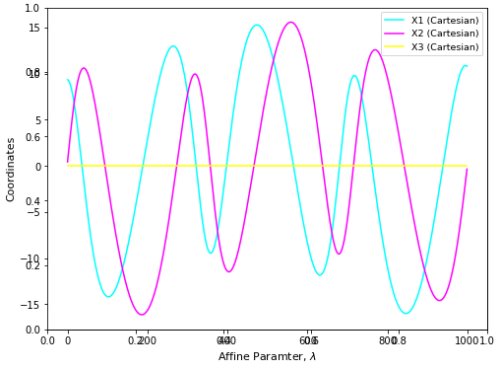

(b) These are the Cartesian values of $(X_1, X_2, X_3) = (x, y, z)$. Note, z is constant as the particle remains on the same plain.

Figure 5.17: The code used to produce the above plots can be found with link to code.

By understanding how to extract the solution provided, one can produce a plot using the standard python library matplotlib.pyplot, among the information from GeodesicPlotter we have the trajectory, which contains the information obtained in Cartesian coordinates of x, y and z. Doing so we obtain the following plots:

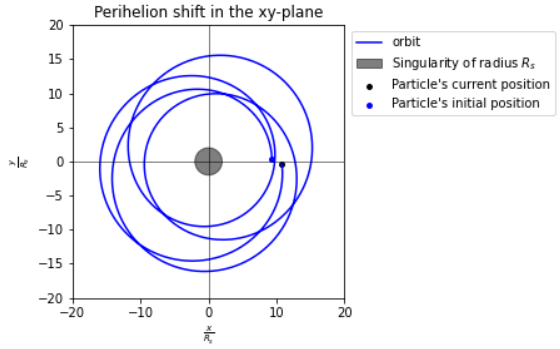

(a) Here we have plotted the massive particle trajectory using matplotlib.pyplot. Compare this plot to Figure 5.13, note the package produces similar results to the RK4 method as expected!

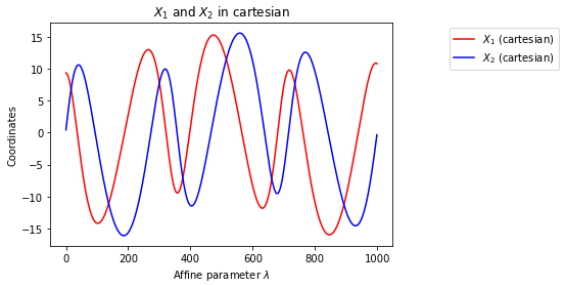

(b) Here we have extracted the information required, from GeoddesicPlotter.trajectory (which is provided as an array of values), to obtain the plot on the left-hand-side.

Figure 5.18: The code used to produce the above plots can be found with link to the code.

Lightlike Geodesic

If we apply the same principle used for the massive particle for photons, i.e. using GeodesicPlotter.trajectory, this time using Nulllike, and particular initial conditions, we obtain the following plots, that will be familiar to you:

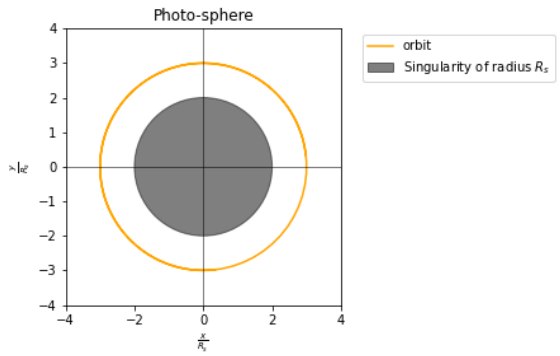

(a) The photo-sphere, compare this to Figure 5.3, see link to code.

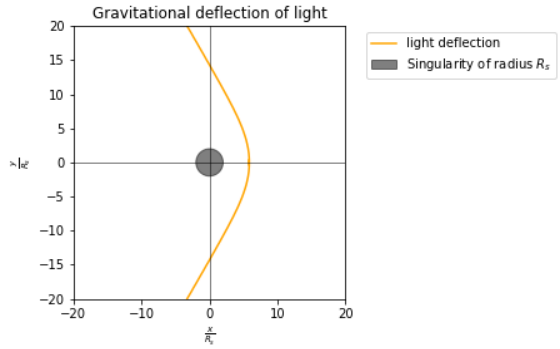

(b) Gravitational deflection of light, compare with Figure 5.6, see link to code.

Figure 5.19: Note, given precise conditions, we have obtained similar plots as before using EinsteinPy, this emphasises the reliability of the package.

In the next section, due to the nature of the problem, we will fully rely on the package to solve the Kerr geodesic, and produce plots of particle trajectory around the Kerr black hole.

5.2 Kerr Geodesic

In this section we are presenting solutions to timelike and lightlike geodesics in the proximity of a Kerr black hole. In particular we are interested in infalling particles, stable orbits and frame dragging of a particle initially spinning in the opposite sense to the angular momentum of the black hole. Starting with:

Stable circular orbit of a massive particle (timelike)

Stable circular orbits around a black hole occurs outside the event horizon but within the ISCO and outside, but not for a black hole with its spin parameter close to its maximum i.e $a = 1$, compare with unstable circular orbit of a Schwarzschild black hole, on the other hand the outermost stable circular orbit (OSCO) [13], at the extreme value of the black hole's angular momentum the radius of OSCO is pushed further away from the black hole. If we now keep the same initial conditions,

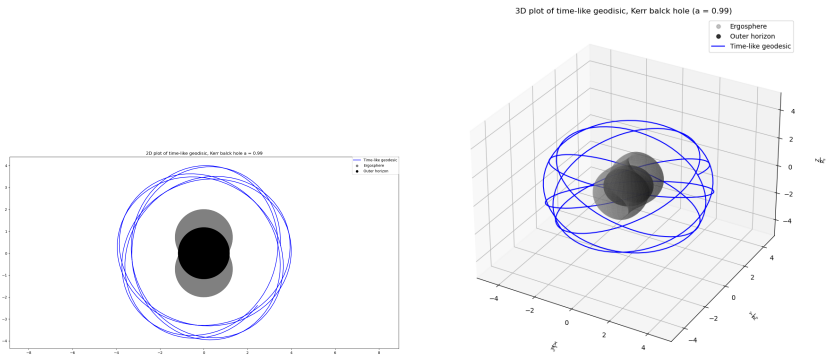

(a) 2D plot, in xy-plane (b) 3D plot

Figure 5.20: The above plots are represent an outermost stable circular orbit as $a = 0.99$, with constant radius $r \approx 2R_s$ (the value fluctuate between ± 0.005). For the input position $= [4, \pi/3, 0]$, momentum $= [0, 0.7679, 2]$, step size delta $= 0.5$ and for 400 steps.

except for the initial radius and increase the accuracy of each steps, i.e. reduce the value of delta, we observe a non-planar perihelion shift.

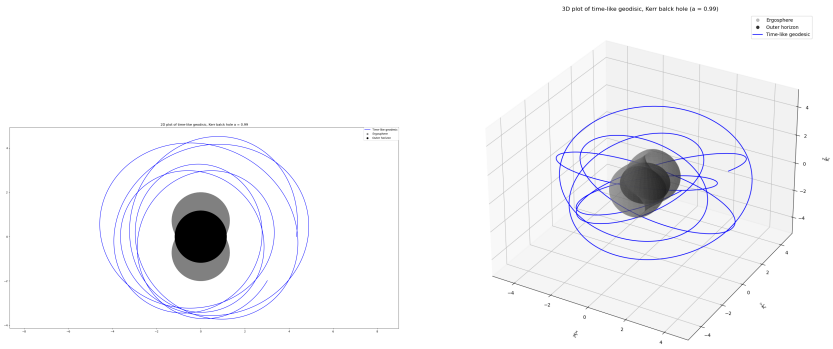

(a) 2D plot, in xy-plane (b) 3D plot

Figure 5.21: Here we kept every condition the same except the initial radius now being $r = 2.5R_s$, and the accuracy of the integration scheme. Do not let the 2D plot convince you that the orbit shrinks down to a smaller orbit, but from the 3D plot it is clear that r is fluctuating between two values $r \in [1.625R_s, 2.5R_s]$. If more steps were used, the perihelion shift would have been more obvious also from he 2D plot.

Infalling particles

As particles fall towards a Kerr black hole, their trajectories are influenced by the black hole's

rotation, leading to distinctive phenomena. Frame dragging causes spacetime to twist, affecting particle motion. Within the ergosphere, particles are forced to rotate with the black hole. Some particles are captured by the black hole's gravitational pull, contributing to accretion disks and emitting radiation. Gravitational redshift and time dilation occur as particles approach the event horizon, leading to observable effects. Quantum effects near the event horizon produce Hawking radiation. Here we have few examples of infalling particles:

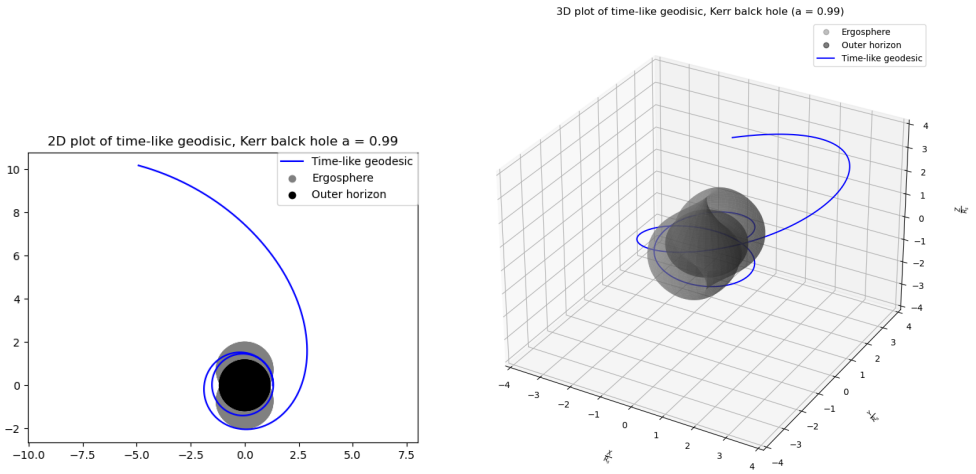

(a) 2D plot, in xy-plane (b) 3D plot

Figure 5.22: This plot was produced by inputting the following parameters, position $= [0.75R_s, \pi/3, 0]$, momentum $= [0, 0.7678, 2]$, delta $= 0.0005$, omega $= 0.01$, and this required 80000 steps.

Frame dragging

To produce plots of frame dragging we will consider the can of initial opposite angular momentum for both lightlike and timelike geodesic (this is particularly important for the Penrose process).

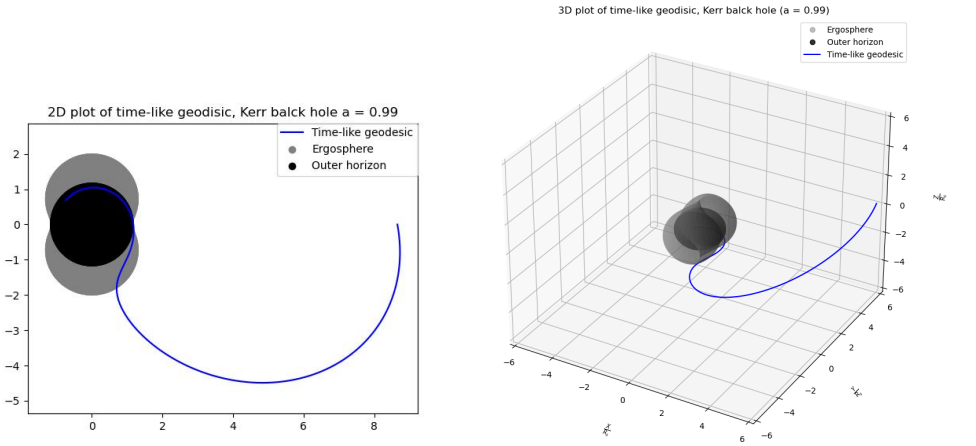

(a) 2D plot, in xy-plane (b) 3D plot

Figure 5.23: position $= [5R_s, \pi/3, 0]$, momentum $= [0, 0.7679, -2]$, delta $= 0.005$, omega $= 0.01$.

We are now going to compare the plots of frame dragging for lightlike geodesics, with the same initial parameters but two different values of a ($a = 0.5, a = 0.99$), to see how the frame dragging effect of light reduces as $a \to 0$ (back to static black hole).

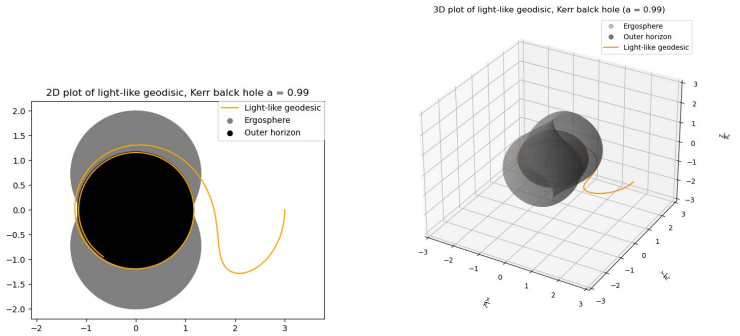

(a) 2D plot, in xy-plane (b) 3D plot

Figure 5.24: Initial conditions, position $= [1.5R_s, \pi/2, 0]$, momentum $= [0, 0, -2]$, delta $= 0.0001$, omega $= 0.01$, steps $= 100000$.

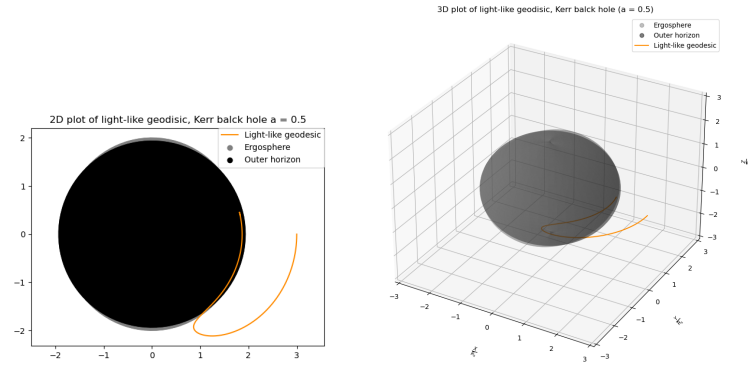

(a) 2D plot, in xy-plane (b) 3D plot

Figure 5.25: Initial conditions, position $= [1.5R_s, \pi/2, 0]$, momentum $= [0, 0, -2]$, delta $= 0.0001$, omega $= 0.01$, steps $= 100000$.

Consider the above Figures (5.24, 5.25), note for both figures the choice of initial condition $r = 1.5R_s$ is not random, in fact at $r = 1.5R_s$ it lies the photosphere, by setting the spin parameter $a = 0$ we get back to the unstable circular orbit, lightlike geodesic, of a Schwarzschild black hole (compare with Figure 5.3). For all the above plots please see codes Kerr_trajectory and Frame_Dragging_Kerr_Black_Hole.

5.3 Penrose Process

The understanding of particle motions around static and rotating black holes, may have other applications, including (theoretically) energy extraction from rotating black holes.

The Penrose process (often referred as Penrose mechanism), proposed by Sir Roger Penrose in 1969 [11, 57, 77, 93], is a theoretical process developed for energy extraction from a rotating black hole (Kerr/Kerr-Newman black hole). This process requires the presence of the ergosphere, hence it could also be applied to rotating stars in the presence of ergosphere. In the process, we send a working body (an unstable particle) towards the ergosphere. Once it reaches the ergosphere, at its lowest point, the body will release a propellant on the opposite direction of the black hole's spin, (from an external observer this will not be recorded due to the frame dragging effect of the ergosphere, i.e. the body still seems to follow the ergosphere). As the propellant slows down it falls to the event horizon, therefore, the remaining part of the body accelerates and gains sufficient speed to escape the ergosphere with excess of energy (which is significantly larger than the loss of energy due to the release of the propellant and the initial energy required to send the body). There is a limit to the amount of energy that can be extracted from a rotating uncharged black hole, assuming the best case of maximal rotation, i.e. $a = 1$, the maximum amount of energy that a single particle can possibly gain decays by the Penrose process is 20.7% of its initial mass. Unfortunately, in stars, the existence of an ergosphere leads to an instability [38]. If we were to send a working body it would be trapped there, and start orbiting the star within the ergoregion making it impossible to escape, requiring more propellant to be released to escape the star leading to a higher demand in energy, contrasting the whole purpose of the Penrose process.

Chapter 6

Conclusion

To conclude, I would like to talk about the truncation error of both numerical integration methods applied throughout the thesis, starting with Runge-Kutta 4 [16, 106] and then moving on to FANTASY[24], so that we can provide a comparison of the two.

Runge-Kutta 4

The truncation error of a numerical method, refers to the error incurred by approximating the solution of a differential equation with a finite number of steps. In the context RK4, it is a fourth order method, meaning that it is designed to approximate the solution of ODEs with an error that is proportional to the step size raised to the power of 5. However, the actual error in each step will be less than the value predicted, dues to error cancellation. In the case of particle's motion in the Schwarzschild black hole this method will provide highly accurate results for the right value step size, in our case the code runs with step size $h = 0.01$, hence we can predict that the error for step size will be $error \leq h^5$ [95], which is enough for the nature of the problem. The truncation error of RK4 can be derived theoretically by comparing the Taylor series expansion of the exact solution with the approximation provided by RK4, i.e. the difference between the exact solution and the approximated solution. Mathematically, if $y(t)$ is the exact analytical solution and y_n is the numerical approximation from RK4 at time t_n, then the truncation error T_n at step n is given by:

$$T_n = y(t_n) – y_n \tag{6.0.0.1}$$

Usually, the truncation error decreases as the step size decreases. This is because a smaller step size means more steps are taken to reach the same final time, and thus the cumulative error is reduced. However, there's a point of diminishing returns was reducing the step size further may not significantly decrease the truncation error due to limitations in numerical precision or rounding errors, but for the chosen step size $h = 0.01$ this problem should not occur, as h is not too small for limitation numerical precision, and not too big for a significant error at each step. Applying these methods is not of our interest.

FANTASY

EinsteinPy [9, 56] has a module dedicated to integration called Integrators. Within Integrators one can find two modules, Runge Kutta module and FANTASY, for all the plots provided using EinsteinPy are coded suing the FANTASY through GeodesicPlotter, which share the same features, but with few differences, of the FANTASY module. This also requires the modules Timelike (massive particles) and Nulllike (photons). As input parameters:

- metric (this is the metric function a user can either select one of the three options, *Schwarzschild, Kerr, and Kerr-Newman*)

- metric_params (spin of the black hole a)
- position and momentum (input of initial position and momentum, but only the spatial coordinates),
- steps (input the number of steps)
- delta (input the step size, default to 0.5, one can reduce it to increase the accuracy of the numerical computation)
- omega (This couples the Hamiltonian flows and the smaller values implying smaller integration error, but if too small it could lead to a non-integrable equation of motion)

What really determines the accuracy of the numerical integration are the step size delta and omega. It is possible to verify the coordinate and based error using the exceptions module. The integration scheme used in FANTASY has an iterative error that goes like $error \leq delta^7$ [24], making the integration scheme from FANTASY more accurate than RK4.

Now the integration scheme used in FANTASY can be very accurate, if appropriate values for delta and omega are chosen, but there is a problem with small values of delta and omega, as we chose small values we need to increase the number of steps the computer needs to process to be able to generate enough data to plot trajectories. In fact to produce Figure 5.21, it took a long time (4 hours and 55 minutes) for the computer to run the code due to the very large amount of steps required ($steps = 2 \times 10^6$), for values of $delta = 0.0001$ and $omega = 0.01$, this plot required a very high computational precision as the objective was to resemble the perihelion shift near a Schwarzschild black hole for a massive particle in a Kerr black hole with spin parameter $a = 0.99$, when using "too large" values of delta the computer was running into severe error, e.g. default value $delta = 0.5$ is too large for this scenario.

The issue we just arised can be approached in different ways, one could write a more sophisticate algorithm that requires less computational power, or one could use more powerful machines such as supercomputers [22] and quantum computers [55]. A supercomputer can perform a quadrilion flops[1] (10^{15}) [34] making a supercomputer one million times more powerful and precise than a commercial laptop. Quantum supremacy [7] is a term in quantum computing that refers to the point where a quantum computer can solve a problem that would be practically impossible for classical computers, either because the problem is too complex or because it would take classical computers an unreasonable amount of time to solve it. It essentially represents the moment when a quantum computer demonstrates its superiority over classical computers in performing a specific task. This achievement is often accompanied by a measurable and significant speedup in computation time compared to the best classical algorithms available. In general a quantum computer can be one hundred million times faster than a regular computer. Regular computers can only exist in two bits 1 and 0, while a quantum computer can be in multiples states at the same time, instead of bits a quantum computer works in qubits denoted as 0 and 1. Hence by using more powerful machines one can obtain more accurate results in significantly less time.

[1] Floating-point operator per second

Bibliography

[1] Benjamin P Abbott et al. "GW150914: The Advanced LIGO detectors in the era of first discoveries". In: *Physical review letters* 116.13 (2016), p. 131103.

[2] Alex Abramovici et al. "LIGO: The laser interferometer gravitational-wave observatory". In: *science* 256.5055 (1992), pp. 325–333.

[3] Fausto Acernese et al. "Virgo status". In: *Classical and Quantum Gravity* 25.18 (2008), p. 184001.

[4] HR Aggarwal and VR Oberbeck. "Roche limit of a solid body". In: *Astrophysical Journal, Vol. 191, pp. 577-588 (1974)* 191 (1974), pp. 577–588.

[5] Paul M Alsing, Jonathan R McDonald, and Warner A Miller. "The simplicial Ricci tensor". In: *Classical and Quantum Gravity* 28.15 (2011), p. 155007.

[6] Georgios Antoniou et al. "Black hole scalarization with Gauss-Bonnet and Ricci scalar couplings". In: *Physical Review D* 104.4 (2021), p. 044002.

[7] Frank Arute et al. "Quantum supremacy using a programmable superconducting processor". In: *Nature* 574.7779 (2019), pp. 505–510.

[8] Ibrahima Bah and Pierre Heidmann. "Geometric resolution of the Schwarzschild horizon". In: *Physical Review D* 109.6 (2024), p. 066014.

[9] Shreyas Bapat et al. "EinsteinPy: a community Python package for general relativity". In: *arXiv preprint arXiv:2005.11288* (2020).

[10] James M Bardeen. "Kerr metric black holes". In: *Nature* 226.5240 (1970), pp. 64–65.

[11] Michał Bejger et al. "Collisional Penrose process near the horizon of extreme Kerr black holes". In: *Physical review letters* 109.12 (2012), p. 121101.

[12] Rachel Berkowitz. "Balding Black Holes Lose Their Magnetic Hair". In: ().

[13] Thomas Berry, Alex Simpson, and Matt Visser. "Photon spheres, ISCOs, and OSCOs: Astrophysical observables for regular black holes with asymptotically Minkowski cores". In: *Universe* 7.1 (2020), p. 2.

[14] F Borkowski et al. "Electromagnetic form factors of the peoton at low four-momentum transfer (II)". In: *Nuclear Physics B* 93.3 (1975), pp. 461–478.

[15] Harvey R Brown. "The origins of length contraction: I. The FitzGerald–Lorentz deformation hypothesis". In: *American Journal of Physics* 69.10 (2001), pp. 1044–1054.

[16] John Butcher. "Runge-kutta methods". In: *Scholarpedia* 2.9 (2007), p. 3147.

[17] Juan Manuel Camacho and Victor Sosa. "Alternative method to calculate the magnetic field of permanent magnets with azimuthal symmetry". In: *Revista mexicana de física E* 59.1 (2013), pp. 8–17.

[18] Bernard J Carr and Stephen W Hawking. "Black holes in the early Universe". In: *Monthly Notices of the Royal Astronomical Society* 168.2 (1974), pp. 399–415.

[19] Sean M Carroll. *Spacetime and geometry*. Cambridge University Press, 2019.

[20] D Chalonge. "Sir Arthur Eddington (1882-1944)". In: *L'Astronomie, vol. 60, pp. 83-85* 60 (1946), pp. 83–85.

[21] Bang-yen Chen and Tadashi Nagano. "Totally geodesic submanifolds of symmetric spaces, I". In: (1977).

[22] Yunji Chen et al. "Dadiannao: A machine-learning supercomputer". In: *2014 47th Annual IEEE/ACM International Symposium on Microarchitecture*. IEEE. 2014, pp. 609–622.

[23] Vladimir A Chobotov. *Orbital mechanics*. Aiaa, 2002.

[24] Pierre Christian and Chi-kwan Chan. "FANTASY: User-friendly Symplectic Geodesic Integrator for Arbitrary Metrics with Automatic Differentiation". In: *The Astrophysical Journal* 909.1 (2021), p. 67.

[25] T Christodoulakis et al. "Conditional symmetries and the canonical quantization of constrained minisuperspace actions: The Schwarzschild case". In: *Journal of Geometry and Physics* 71 (2013), pp. 127–138.

[26] Demetrios Christodoulou. *The action principle and partial differential equations*. 146. Princeton University Press, 2000.

[27] Colin W Cryer and Lucio Tavernini. "The numerical solution of Volterra functional differential equations by Euler's method". In: *SIAM Journal on Numerical Analysis* 9.1 (1972), pp. 105–129.

[28] Thibault Damour. "Testing the equivalence principle: why and how?" In: *Classical and Quantum Gravity* 13.11A (1996), A33.

[29] Thibault Damour. "Theoretical aspects of the equivalence principle". In: *Classical and Quantum Gravity* 29.18 (2012), p. 184001.

[30] Lieven De Lathauwer, Bart De Moor, and Joos Vandewalle. "A multilinear singular value decomposition". In: *SIAM journal on Matrix Analysis and Applications* 21.4 (2000), pp. 1253–1278.

[31] Frank Watson Dyson, Arthur Stanley Eddington, and Charles Davidson. "IX. A determination of the deflection of light by the Sun's gravitational field, from observations made at the total eclipse of May 29, 1919". In: *Philosophical Transactions of the Royal Society of London. Series A, Containing Papers of a Mathematical or Physical Character* 220.571-581 (1920), pp. 291–333.

[32] Albert Einstein. "The Bianchi identities in the generalized theory of gravitation". In: *Canadian Journal of Mathematics* 2 (1950), pp. 120–128.

[33] Ernesto F Eiroa, Gustavo E Romero, and Diego F Torres. "Reissner-Nordström black hole lensing". In: *Physical Review D* 66.2 (2002), p. 024010.

[34] Michael J Ellsworth Jr et al. "An overview of the IBM power 775 supercomputer water cooling system". In: (2012).

[35] Myron W Evans et al. *Criticisms of the Einstein Field Equation*. 2011.

[36] CW Francis Everitt et al. "Gravity probe B: final results of a space experiment to test general relativity". In: *Physical Review Letters* 106.22 (2011), p. 221101.

[37] Matthew R Francis and Arthur Kosowsky. "Geodesics in the generalized Schwarzschild solution". In: *American journal of physics* 72.9 (2004), pp. 1204–1209.

[38] John L Friedman. "Ergosphere instability". In: *Communications in Mathematical Physics* 63.3 (1978), pp. 243–255.

[39] Pierre Fromholz, Eric Poisson, and Clifford M Will. "The Schwarzschild metric: It's the coordinates, stupid!" In: *American Journal of Physics* 82.4 (2014), pp. 295–300.

[40] Chris L Fryer and Kimberly CB New. "Gravitational waves from gravitational collapse". In: *Living Reviews in Relativity* 14 (2011), pp. 1–93.

[41] Forshaw Smith & Jeffrey Gavin. *Dynamics and Relativity*. John Wiley & Sons, 2014.

[42] Sushant G Ghosh, Muhammed Amir, and Sunil D Maharaj. "Ergosphere and shadow of a rotating regular black hole". In: *Nuclear Physics B* 957 (2020), p. 115088.

[43] Norman Gürlebeck. "No-hair theorem for black holes in astrophysical environments". In: *Physical Review Letters* 114.15 (2015), p. 151102.

[44] Eva Hackmann and Claus Lämmerzahl. "Geodesic equation in Schwarzschild-(anti-) de Sitter space-times: Analytical solutions and applications". In: *Physical Review D* 78.2 (2008), p. 024035.

[45] Andrew JS Hamilton. "Interior structure of rotating black holes. II. Uncharged black holes". In: *Physical Review D* 84.12 (2011), p. 124056.

[46] Stephen W Hawking. "Black holes in general relativity". In: *Communications in Mathematical Physics* 25 (1972), pp. 152–166.

[47] Seyed Hossein Hendi. "Asymptotic Reissner–Nordström black holes". In: *Annals of Physics* 333 (2013), pp. 282–289.

[48] Ibrar Hussain and Sajid Ali. "Marginally stable circular orbits in the Schwarzschild black hole surrounded by quintessence matter". In: *The European Physical Journal Plus* 131.8 (2016), p. 275.

[49] Maximiliano Isi et al. "Testing the no-hair theorem with GW150914". In: *Physical Review Letters* 123.11 (2019), p. 111102.

[50] Savitri V Iyer and Arlie O Petters. "Light's bending angle due to black holes: from the photon sphere to infinity". In: *General Relativity and Gravitation* 39 (2007), pp. 1563–1582.

[51] Griffiths David J. *Electrodynamics and Relativity, Chapter 12*. Pearson, 4th ed, 2013.

[52] Oleg D Jefimenko. "On the experimental proofs of relativistic length contraction and time dilation". In: *Zeitschrift für Naturforschung A* 53.12 (1998), pp. 977–982.

[53] VM Khatsymovsky. "On the discrete Christoffel symbols". In: *International Journal of Modern Physics A* 34.30 (2019), p. 1950186.

[54] Tamara G Kolda and Brett W Bader. "Tensor decompositions and applications". In: *SIAM review* 51.3 (2009), pp. 455–500.

[55] Thaddeus D Ladd et al. "Quantum computers". In: *nature* 464.7285 (2010), pp. 45–53.

[56] Jose Miguel Ladino, Carlos Andrés del Valle, and Eduard Larrañaga. "Motion of Spinning Particles around Black Holes". In: *arXiv preprint arXiv:2302.12352* (2023).

[57] J-P Lasota et al. "Extracting black-hole rotational energy: The generalized Penrose process". In: *Physical Review D* 89.2 (2014), p. 024041.

[58] Anthony R Lee and Tomas M Kalotas. "Lorentz transformations from the first postulate". In: *American Journal of Physics* 43.5 (1975), pp. 434–437.

[59] José PS Lemos and Diogo LFG Silva. "Maximal extension of the Schwarzschild metric: from Painlevé–Gullstrand to Kruskal–Szekeres". In: *Annals of Physics* 430 (2021), p. 168497.

[60] Gilbert N Lewis. "The symmetry of time in physics". In: *Science* 71.1849 (1930), pp. 569–577.

[61] JC Ling et al. "The states of Cygnus X-1". In: *Astrophysical Journal, Part 1 (ISSN 0004-637X), vol. 275, Dec. 1, 1983, p. 307-315. NASA-supported research.* 275 (1983), pp. 307–315.

[62] Florian Loebbert et al. "Three-body effective potential in general relativity at second post-Minkowskian order and resulting post-Newtonian contributions". In: *Physical Review D* 103.6 (2021), p. 064010.

[63] Anatoly A Logunov. "Henri Poincaré and relativity theory". In: *arXiv preprint physics/0408077* (2004).

[64] David Lovelock. "The Einstein tensor and its generalizations". In: *Journal of Mathematical Physics* 12.3 (1971), pp. 498–501.

[65] David Lovelock. "The four-dimensionality of space and the Einstein tensor". In: *Journal of Mathematical Physics* 13.6 (1972), pp. 874–876.

[66] David Lovelock. "The uniqueness of the Einstein field equations in a four-dimensional space". In: *Archive for Rational Mechanics and Analysis* 33 (1969), pp. 54–70.

[67] Mark Lutz. *Programming python.* " O'Reilly Media, Inc.", 2001.

[68] David B Malament. "A remark about the "geodesic principle" in general relativity". In: *Analysis and interpretation in the exact Sciences: Essays in honour of William Demopoulos.* Springer, 2012, pp. 245–252.

[69] Karl Martel. "Gravitational waveforms from a point particle orbiting a Schwarzschild black hole". In: *Physical Review D* 69.4 (2004), p. 044025.

[70] William D Metz. "Astrophysics: discovery and the ubiquity of black holes". In: *Science* 195.4275 (1977), pp. 276–277.

[71] Edward Arthur Milne. "On the conservation of momentum". In: *Proceedings of the Royal Society of London. Series A. Mathematical and Physical Sciences* 186.1007 (1946), pp. 432–442.

[72] Akash K Mishra, Sumanta Chakraborty, and Sudipta Sarkar. "Understanding photon sphere and black hole shadow in dynamically evolving spacetimes". In: *Physical Review D* 99.10 (2019), p. 104080.

[73] G Mustafa and Ibrar Hussain. "Radial and circular motion of photons and test particles in the Schwarzschild black hole with quintessence and string clouds". In: *The European Physical Journal C* 81.5 (2021), p. 419.

[74] Igor'dmitrievich Novikov and VALERYP Frolov. *Physics of black holes.* Vol. 27. Springer Science & Business Media, 2013.

[75] Donald Ornstein. "Dual vector spaces". In: *Annals of Mathematics* 69.3 (1959), pp. 520–534.

[76] Jerome A Orosz et al. "The mass of the black hole in Cygnus X-1". In: *The Astrophysical Journal* 742.2 (2011), p. 84.

[77] Robert F Penna. "Energy extraction from boosted black holes: Penrose process, jets, and the membrane at infinity". In: *Physical Review D* 91.8 (2015), p. 084044.

[78] Herbert Pfister. "On the history of the so-called Lense-Thirring effect". In: *General Relativity and Gravitation* 39 (2007), pp. 1735–1748.

[79] Souvik Pramanik. "Implication of the geodesic equation in the generalized uncertainty principle framework". In: *Physical Review D* 90.2 (2014), p. 024023.

[80] Gabriel A Radvansky. "Across the event horizon". In: *Current Directions in Psychological Science* 21.4 (2012), pp. 269–272.

[81] BS Madhava Rao. "Ring-singularity in Born's unitary theory—I". In: *Proceedings of the Indian Academy of Sciences-Section A*. Vol. 4. Springer India. 1936, pp. 355–376.

[82] Christopher S Reynolds. "Observing black holes spin". In: *Nature Astronomy* 3.1 (2019), pp. 41–47.

[83] W Rindler. "Hyperbolic motion in curved space time". In: *Physical Review* 119.6 (1960), p. 2082.

[84] Sebastian Schuster and Matt Visser. "Boyer-Lindquist space-times and beyond: Meta-material analogues". In: *arXiv preprint arXiv:1802.09807* (2018).

[85] Bernard Schutz. *A First Course in GENERAL RELATIVITY*. Cambridge University Press, 3rd ed, 2022.

[86] Bernard F Schutz Jr. "Perfect fluids in general relativity: velocity potentials and a variational principle". In: *Physical Review D* 2.12 (1970), p. 2762.

[87] Karl Friedrich Siburg. *The principle of least action in geometry and dynamics*. 1844. Springer Science & Business Media, 2004.

[88] Pierre Sikivie. "Caustic ring singularity". In: *Physical Review D* 60.6 (1999), p. 063501.

[89] Hans Stephani et al. *Exact solutions of Einstein's field equations*. Cambridge university press, 2009.

[90] Saul A Teukolsky. "The kerr metric". In: *Classical and Quantum Gravity* 32.12 (2015), p. 124006.

[91] Kip S Thorne. "Gravitational waves". In: *arXiv preprint gr-qc/9506086* (1995).

[92] Keith John Treschman. "Early astronomical tests of general relativity: the anomalous advance in the perihelion of Mercury and gravitational redshift". In: *Asian Journal of Physics* 23.1-2 (2014), pp. 171–188.

[93] Arman Tursunov and Naresh Dadhich. "Fifty years of energy extraction from rotating black hole: revisiting magnetic Penrose process". In: *Universe* 5.5 (2019), p. 125.

[94] Anatoli A Vankov. "General Relativity Problem of Mercury's Perihelion Advance Revisited". In: *arXiv preprint arXiv:1008.1811* (2010).

[95] James Hamilton Verner. "Explicit Runge–Kutta methods with estimates of the local truncation error". In: *SIAM Journal on Numerical Analysis* 15.4 (1978), pp. 772–790.

[96] CV Vishveshwara. "Stability of the Schwarzschild metric". In: *Physical Review D* 1.10 (1970), p. 2870.

[97] CV Vishveshwara. "Stability of the Schwarzschild metric". In: *Physical Review D* 1.10 (1970), p. 2870.

[98] GE Volovik. “From black hole to white hole via the intermediate static state”. In: *Modern Physics Letters A* 36.17 (2021), p. 2150117.

[99] Robert M Wald and Andreas Zoupas. “General definition of “conserved quantities” in general relativity and other theories of gravity”. In: *Physical Review D* 61.8 (2000), p. 084027.

[100] Johan Walrave. “Curves and surfaces in Minkowski space”. In: (1995).

[101] Clifford M Will. “The 1919 measurement of the deflection of light”. In: *Classical and Quantum Gravity* 32.12 (2015), p. 124001.

[102] Joseph A Wolf. “Growth of finitely generated solvable groups and curvature of Riemannian manifolds”. In: *Journal of differential Geometry* 2.4 (1968), pp. 421–446.

[103] Bing Zhang, Shiho Kobayashi, and Peter Mészáros. “Gamma-ray burst early optical afterglows: implications for the initial Lorentz factor and the central engine”. In: *The Astrophysical Journal* 595.2 (2003), p. 950.

[104] Jingyi Zhang and Zheng Zhao. “Charged particles’ tunnelling from the Kerr–Newman black hole”. In: *Physics Letters B* 638.2-3 (2006), pp. 110–113.

[105] Jingyi Zhang and Zheng Zhao. “New coordinates for Kerr–Newman black hole radiation”. In: *Physics Letters B* 618.1-4 (2005), pp. 14–22.

[106] David W Zingg and Todd T Chisholm. “Runge–Kutta methods for linear ordinary differential equations”. In: *Applied Numerical Mathematics* 31.2 (1999), pp. 227–238.